Hot Spots

13

13.1 Introduction

Hot spots are the surface expression of plumes of hotter and lighter material upwelling from the Earth's mantle. The current number of hot spots is estimated to range between 45 and 70: these are mostly in intraplate settings, especially on oceanic lithosphere, and along divergent plate boundaries. Neglecting hot spots along divergent boundaries and shaped by the related far-field tectonics (as with Afar and Iceland, described in Chap. 11), oceanic hot spot volcanoes show a considerable variability in distribution, evolution and activity, as at Hawaii, Galapagos, Easter Island, Reunion, Canary Islands and Azores. This results from the different mantle plume properties (plume configuration and productivity) and local tectonic context (age of the intruded oceanic lithosphere, rate of plate motion, pre-existing structures), which make each hot spot distinctive. Despite this variability, most oceanic hot spot volcanoes also display recurrent structural features, which include overlapping mafic edifices with summit calderas, radial volcanic rift zones and flank instability. Then, there is the less common and more evolved volcanism derived from continental hot spots, of which Yellowstone is the most dramatic example and, at the same time, quite distinct from other less productive continental cases, as for instance Tibesti. All these characteristics make hot spots widely different, stimulating from structural and magmatic perspectives and complicating established models.

This chapter considers examples from oceanic and, subordinately, continental hot spots. In the Pacific Ocean region, three very different types of hot spots are considered: Hawaii, Galapagos and Easter Island. Then, in the Indian Ocean region the productive Reunion hot spot is presented. Subsequently, in the Atlantic Ocean region, the different hot spots of the Canary Islands and the Azores are considered. Finally, the different features of the continental Yellowstone and Tibesti hot spots are presented.

The main aims of this chapter are:

- first to define the primary structural and magmatic characters of hot spot activity, describing representative oceanic and continental cases;
- second to provide a general framework summarizing the structural and magmatic features of hot spot volcanoes, with a working hypothesis for oceanic types.

13.2 Hawaii Hot Spot

The Hawaiian plume is imaged as a continuous low velocity anomaly from the base of the mantle to the surface. Its shallowest part may consist of discrete portions, diapirs, plumelets or filaments, with radii of $\sim$10 km and heights $\sim$100 km.

V. Acocella, *Volcano-Tectonic Processes*, Advances in Volcanology,
https://doi.org/10.1007/978-3-030-65968-4_13

Ascending mantle diapirs may be sheared by the differential motion between the upper mantle and the lithosphere. The shallow plume contains a melt-rich zone 110–155 km beneath Hawaii Island, whose axial region is a mixture of recycled subducted components and primitive lower mantle materials, implying spatial heterogeneity. The plume outside the head region, inferred to lie beneath the southeast coast of Hawaii Island, is less heterogeneous but distinct from the upper mantle (Wolfe et al. 2009; Farnetani and Hoffmann 2010; Rychert et al. 2013).

The ~6000 km long Hawaiian-Emperor volcanic chain marks the surface trace of the plume, consisting of at least 107 volcanoes with volume of ~1 million km^3 (Fig. 13.1a). Individual seamounts along the chain may be the topographic expression of discrete diapirs from a single deeper mantle plume. The chain is age progressive, with active volcanoes at the southeast end and 75–80 Ma old volcanoes at the northwest end. The bend between the Hawaiian and Emperor chains reflects a major change in Pacific plate motion at ~47 Ma. Age-distance data along the chain also reflect minor deviations from an overall linear trend. Volume calculations highlight an increase in the hot spot activity since 30 Ma and especially during the last 1 Ma (Fig. 13.1b; Vidal and Bonneville 2004; Robinson and Eakins 2006; Sharp and Clague 2006).

The Hawaiian volcanoes undergo progressive subsidence and erosion as they move farther from the hot spot, becoming drowned islands or seamounts. The subsidence results from the load on the lithosphere due to the growing volcanoes, which causes the lithosphere to sag and the Hawaiian Ridge to subside. Superimposed is the subsidence caused by the thermal contraction of the aging oceanic lithosphere, which becomes older westwards. Most volcanoes have subsided 2–4 km since reaching the sea surface, while their bases have subsided 5–8 km, so that about half of the construction of the volcanoes is reduced by subsidence. The bulk of the subsidence is complete ~1 Ma after initiation of volcanism on the seafloor. Overall, the observed rates of vertical motion of the islands adequately record the flexural response of the lithosphere to volcanic loads (Moore 1987; Huppert et al. 2015).

Hawaiian volcanoes contain intrusions estimated at less than 30% by volume, indicating that the edifices are predominately built extrusively. Edifice building has involved four major growth stages. The earliest is the submarine alkalic preshield stage, before the development of a shield volcano. The alkalic composition derives from a nascent magma-transport system and less extensive melting at the plume periphery. The subsequent tholeiitic shield stage accounts for more than 95% of the volume and may be ~1 Ma long. This marks the time when a volcano is near or above the hot spot and its robust magma supply system builds the shield, which mainly consists of tholeiitic basalts and subordinate basalt andesites. Volcanism wanes as the volcano moves away from the hot spot, passing into the post-shield stage. Shallow magma reservoirs (1–7 km depth) cannot be sustained, as magma supply lessens, but reservoirs at 20–30 km depth persist. The rate of extrusion diminishes by a factor of 10 and lavas become more alkalic, eventually evolving to trachytic compositions, as the degree of melting diminishes. Therefore, a cap of alkalic basalt and associated differentiates covers the tholeiitic shield (Lipman and Calvert 2013; Clague and Sherrod 2014). After several million years of erosion, alkalic rejuvenated-stage magma may erupt from isolated vents as the volcanoes override the moat flexure created by loading and subsidence of the new shield volcano lying southeast on the chain. The rejuvenated onshore and offshore volcanism may be partly explained by the enhanced rupture of the oceanic lithosphere in its flexural uplift zone, producing focused magmatic fluxes over an area two to ten times the eruption area. Five Hawaiian volcanoes contain rejuvenated-stage volcanism following quiescent periods that range from 2 to less than 0.5 Ma (Bianco et al. 2005; Thordarson and Garcia 2018, and references therein). Such a prolonged construction of the Hawaiian shields has been also often punctuated by giant and rapid landslides, with seventeen discrete large slides forming around the main islands in the past 5 Ma.

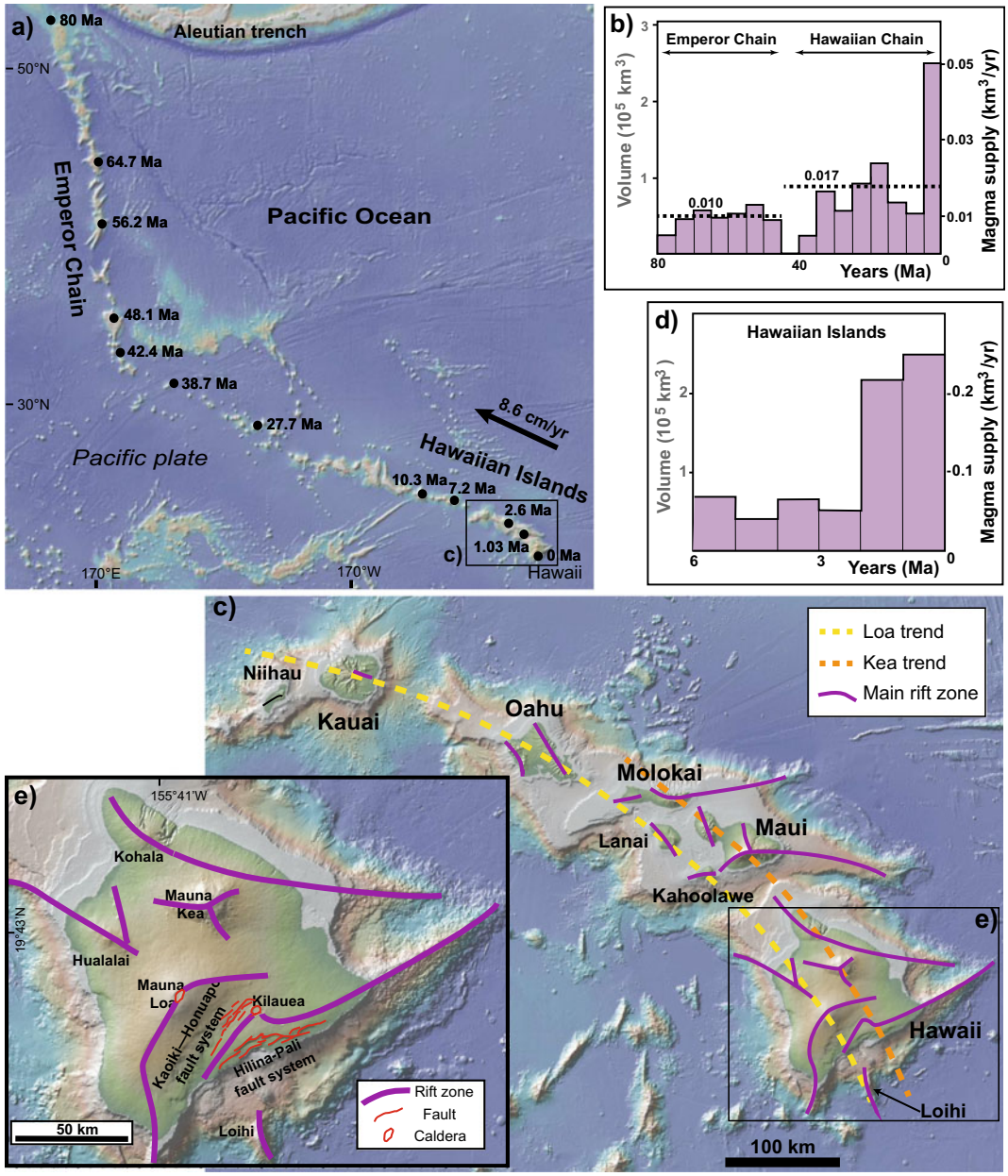

Fig. 13.1 Hawaii hot spot. **a** Overview of the Hawaii-Emperor Chain, resulting from the activity of the Hawaiian plume; plate velocity is relative to the hot spot; **b** related variation of the volcano volumes with time. **c** Overview of the Hawaiian Islands, with the "Kea" and "Loa" trends and the main volcanic rift zones; inset **d** shows the related variation of the erupted volumes with time (Robinson and Eakins 2006). **e** Overview of the subaerial and submarine portions of the island of Hawaii, its volcanoes, rift zones and main fault systems. Digital Elevation Models provided by GeoMapApp

Volcanic centres on the Hawaiian Ridge follow two curved loci roughly parallel to the ridge and ~40 km apart, forming the "Loa" and "Kea" subchains, with geochemical variations reflecting preferential sampling of two distinct sources of deep mantle material. These loci may mark the edges of downbending of the two sides of the lithospheric subsidence trough, where fracturing conducts magma to the surface. The progressive involvement of the "Loa" component, as recorded in the magma erupted since ~6.5 Ma, records the strengthening of the Hawaiian plume through time (Fig. 13.1c; Moore 1987; Weis et al. 2011; Harrison et al. 2017). The volcanoes of the Hawaiian Islands become progressively younger southeastwards, from Kauai (3.9–5.8 Ma) to Hawaii (<1 Ma). Hawaii, the largest of the Hawaiian Islands, has grown at an average rate of ~10^5 km^3/Ma and is presently close to its maximum size. Subaerial Hawaii Island consists of five coalesced and overlapping volcanoes which have formed in the past 1 Ma: Kohala, Hualalai, Mauna Kea, Mauna Loa and Kilauea. Each of these volcanoes requires approximately 600 ka to grow from the ocean floor to the end of shield building stage, reaching the ocean surface about midway (Fig. 13.1e). Kohala completed shield building at ~245 ka, Hualalai and Mauna Kea at 130 ka. Mauna Kea, the tallest volcano, last erupted at ~4.5 ka. It is capped by alkalic lava flows modifying the original shield, and it is uncertain if a summit caldera and well-defined volcanic rift zones existed. Although tall, Mauna Kea may have a modest volume, as its edifice appears perched on the flank of Kohala (Moore and Clague 1992; Lipman and Calvert 2013; Clague and Sherrod 2014; Poland et al. 2014, and references therein). Mauna Loa is the largest volcano, showing shield stage tholeiitic lava mostly issued from the summit and southwest and northeast rift zones, although radial eruptive fissures also exist on its western and northern flanks (Fig. 13.2). Eruptive activity ranges from at least 700 ka to 1984 AD. The current summit magma system includes two interconnected reservoirs, with one centred beneath the south caldera

Fig. 13.2 Hawaii hot spot. Summit of Mauna Loa volcano viewed from the south, showing the caldera with the 1940 eruptive vent. The eruptive fissure and linear vents in the foreground are the proximal part of the Southwest Rift, and the summit of nearby Mauna Kea volcano is partly visible in the background. *Photo credit* U.S. Geological Survey, USGS

margin and the other elongated along the caldera axis (Poland et al. 2014, and references therein). Kilauea is the youngest and most active volcano of Hawaii. It consists of shield stage tholeiitic lava issued from the summit caldera, as well as the east and southwest rift zones since ~100 ka. The present caldera formed at ~1500 AD, with the subsequent 300 years characterized by highly explosive activity (Langenheim and Clague 1987). Whether or not magma is present along and within the deep rift zone, which extends from beneath the shallower rift at ~3 km depth to the base of the volcano at ~9 km depth, remains an open question. It is probable that most magma entering Kilauea passes through the summit reservoir system before entering the rift zones. The connectivity between the distal rift zones and the summit magma chamber of Kilauea has been observed during several eruptions and further confirmed in 2018, when lateral magma propagation and eruption along the East Rift Zone was accompanied by summit caldera collapse (see Sects. 5.10.3 and 6.7; Okubo et al. 1997; Poland et al. 2014; Clague and Sherrod 2014; Neal et al. 2019; Wauthier et al. 2019).

The active submarine volcano of Loihi, 30 km southeast of Hawaii, is the latest activity of the Hawaiian hot spot. The NNW-SSE striking edifice is ~30 km long and 3 km high. The summit has a caldera-like depression, hosting pit craters and a resurgent block above a magma chamber lying between 1 and 2 km of depth. The volcano taps a relatively primitive part of the plume, producing a wide range of magma compositions reflecting increasing degrees of partial melting as it drifts toward the hot spot centre (Clague et al. 2019, and references therein).

Volcanic rift zones are integral structural elements of Hawaiian volcanoes, consisting of narrow (related vents stretch across most less than 2 km) and long (some more than 100 km) portions of focused volcanic and tectonic activity, including spatter cones, spatter ramparts, pit craters, extension fractures, faults, grabens and eruptive fissures (Fig. 13.3).

Fig. 13.3 Hawaii hot spot. Detail of eruptive fissure developed along the Eastern Rift Zone of Kilauea on March 2011: lava pours from the fissure just after daybreak and cascades out of sight into a deep crack; geologist in yellow circle for perspective. *Photo credit* U. S. Geological Survey, USGS

At depth, the rift zones consist of a thick, subvertical dike-like magma system, where dikes are usually intruded laterally from a central magma reservoir, propagating up to several tens of kilometres without erupting (Fig. 13.4; Delaney et al. 1990). The orientation of the rift zones depends on the presence of regional structures and the local stress field. The long east trending rift zones of Hawaiian volcanoes may follow regional fractures in oceanic crust activated by arching of the Hawaiian swell in front of the propagating hot spot. At volcanoes that grew on the flanks of an already existing edifice, the orientation of rift zones is influenced by the gravitational stress field resulting from the buttressing conditions of the older volcano. In the case of Kilauea, growing on the flank of Mauna Loa, the rift zones are oriented perpendicular to the direction of least buttressing, imposed by the oceanic abyssal plain to the southeast (Fiske and Jackson 1972; Walter et al. 2006; Lipman and Calvert 2011). Loihi does not follow this behaviour, as its NNW-SSE trending rift zone suggests a formation beyond the influence of the gravitational load of the adjacent older volcanoes, probably influenced by the flexure of the lithosphere (Garcia et al. 2006).

The stresses on the volcano flanks also develop large-scale landslides related to the activity of the rift zones, especially the East Rift Zone of Kilauea. The 1975 magnitude *M7.7* and 2018 *M6.9* earthquakes along the detachment at the base of the southern flank of Kilauea likely resulted from the stress induced by overpressured dikes intruded in the rift zone (Swanson et al. 1976; Chen et al. 2019). Both earthquakes produced an abrupt southward movement of the south flank across the underlying oceanic crust, activating the Hilina-Pali normal fault system, which represents the surface expression of the

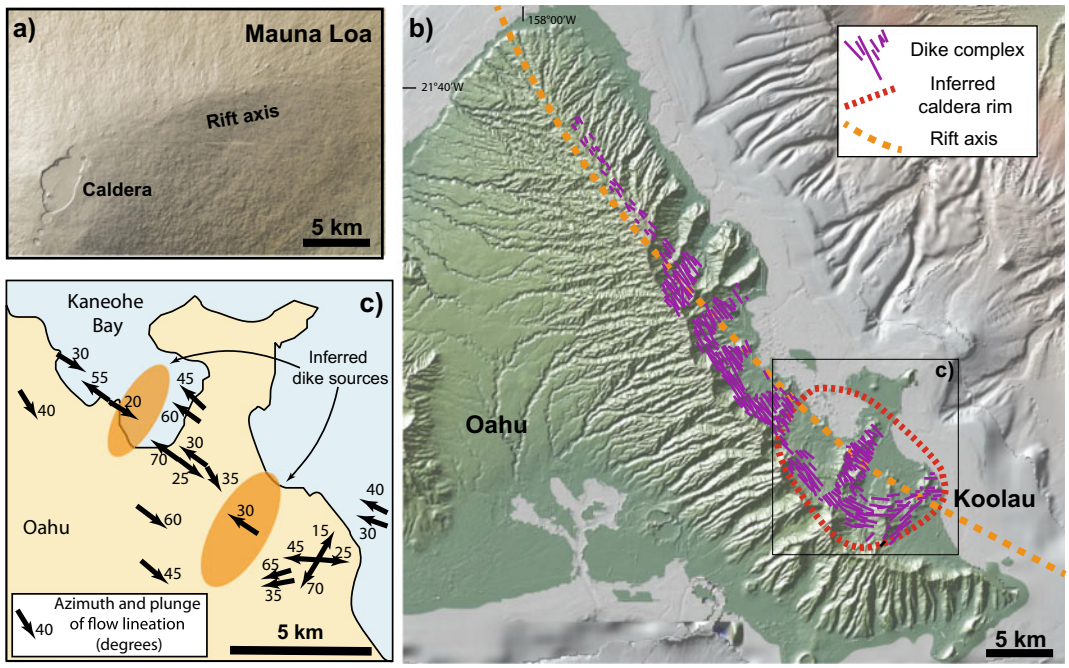

Fig. 13.4 Hawaii hot spot. Comparison between the morphology and structure of active **a** and eroded **b** Hawaiian rift zones, shown at the same scale for comparison. **a** Morphology at the surface of the Northeast Rift of Mauna Loa radiating from the summit caldera and consisting of multiple eruptive fissures at the surface. **b** Deeper structure of the eroded Koolau rift zone, northeast Oahu, at ~1 km depth. **c** Measured directions and plunge of magmatic flow within the dikes along the Koolau rift zone beneath the eroded caldera (Walker 1987). Digital Elevation Models provided by GeoMapApp

instability of this flank (Fig. 13.1e). Such faulting not only provides a means for the flanks to adjust continuously to intrusions, but also contributes to the stress field that encourages dikes to propagate along the rift zone, with dike intrusion and lateral spreading being major contributors to the growth of the volcano (Peterson and Moore 1987; Dieterich 1988; Wang et al. 2019). In addition to Kilauea, Mauna Loa is inferred to have undergone volcano spreading during its early growth, activating the Kaoiki–Honuapo fault system (analogue of the Hilina-Pali fault system on Kilauea; Fig. 13.1e). Cumulative deformation of Mauna Loa's south flank during growth of Kilauea since 200–300 ka involved more than 10 km of seaward spreading, displacing the rift zones of Kilauea, while its deep plumbing system and summit magma reservoir remained nearly fixed; such an evolution also accounts for the arcuate strike of the rift zones of Kilauea (Lipman et al. 2006).

13.3 Galapagos Hot Spot

The Galapagos Archipelago lies in the eastern Pacific Ocean, 200–300 km south of the Galapagos Spreading Ridge that separates the Nazca (to the south) and Cocos plates (Fig. 13.5). The Galapagos Ridge first migrated to the northern edge of the hot spot at 19.5 Ma, overlying the hot spot between 19.5 and 14.5 Ma and then to the south of the hot spot at 14.5 Ma. This split the paleo-Carnegie Ridge into the present Carnegie and Malpelo ridges, with new seafloor separating the two ridges on the Nazca and Cocos plates, respectively. Between 12 and 11 Ma, a later ridge jump shifted the spreading axis north of the hot spot, while spreading between the Carnegie and Malpelo ridges continued until 9.5 Ma (Werner et al. 2003).

Beneath the western Galapagos Archipelago, the thinning of the upper mantle transition zone, between 410 and 660 km depth, within an area

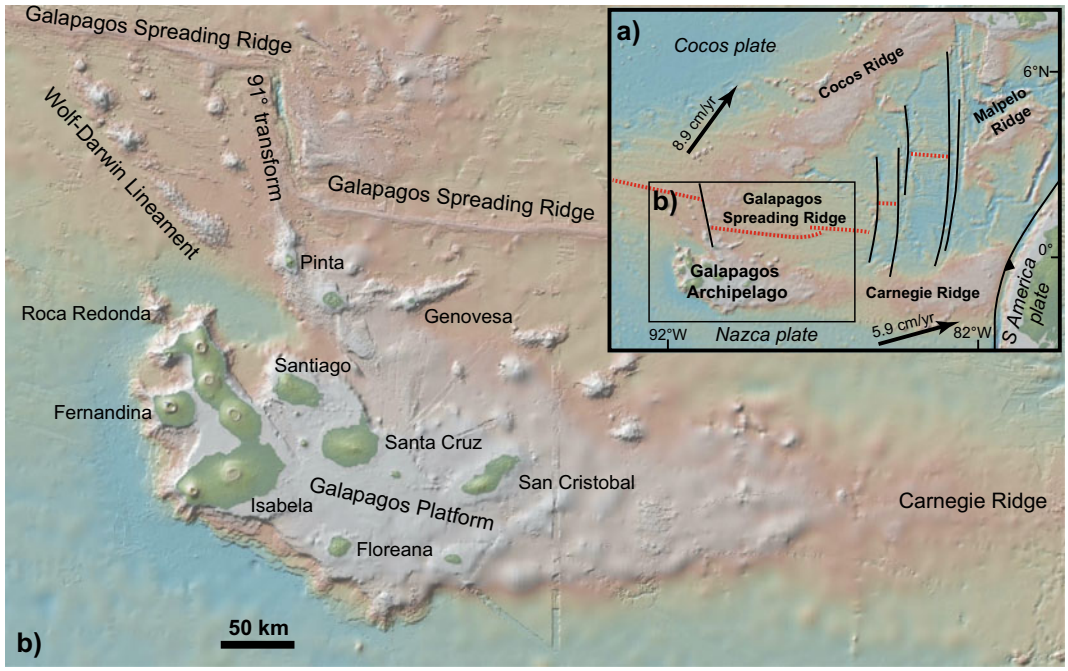

Fig. 13.5 **a** Tectonic setting of the Galapagos hot spot, with the velocities of the plates relative to the hot spot. **b** Overview of the Galapagos Archipelago and the nearby spreading ridge. Digital Elevation Models provided by GeoMapApp

~100 km wide southwest of Fernandina Island, suggests plume upwelling below 410 km. The upper 300 km of the mantle beneath the archipelago contain a low velocity anomaly tilted towards the Galapagos Ridge. At depths of less than 100–120 km, the plume spreads both toward and against eastward plate motion. The plume top is centred near Fernandina (Villagomez et al. 2014). The thickness of the high velocity lithospheric mantle above the plume varies from ~60 km beneath the southwest part of the archipelago to ~45 km below the northeast part. The thicker-than-normal lithosphere to the southwest may result from the residuum from hot spot melting. The thinner lithosphere to the northeast, combined with the lateral deflection of the plume, results in volcanism scattered over a relatively large area. Indeed, the general eastward increase in age of lavas from seamounts, consistent with a hot spot model for their generation, is accompanied by dispersed volcanism, observed also in the distribution of the active volcanoes. In particular, the construction of seven simultaneously active volcanoes indicates that the western Galapagos Islands of Fernandina and Isabela do not result from a simple progression of the lithosphere over a narrowly focused mantle plume. The result is that, while the eruption rate of the Galapagos plume (10^3 km^3/Ma) is smaller than that of the Hawaiian one, active volcanism is more widespread (~40,000 km^2) than in Hawaii (~20,000 km^2; Sinton et al. 1996; Canales et al. 2002; Rychert et al. 2014; Sinton et al. 2018).

The Galapagos Islands stand on a broad volcanic platform lying on young (<10 Ma) oceanic lithosphere. This platform is the shallowest portion of the Carnegie Ridge, whose post-9.5 Ma construction results from the passage of the Nazca plate over the hot spot. The Galapagos platform consists of several tens of large, stepped submarine terraces between 800 and 3500 m depth, sloping outward at less than 2° and surrounded by ~300 m high escarpments with slopes of ~24°. Each terrace results from a sequence of major submarine eruptions, suggesting episodic magma supply. In the western Galapagos, characterized by the currently most active Isabela and Fernandina islands, the platform may have formed in the last ~3 Ma, younging westward and just predating the development of the overlying shield edifices (Geist et al. 2008).

The active volcanoes of the western Galapagos overlying the mantle plume in Isabela and Fernandina islands display a distinctive morphological feature. This consists of the abrupt steepening of their subaerial slope, which passes on average from less than 10° in the distal area to more than 10° and, locally, more than 30°, in the proximal area, giving these volcanoes an "inverted soup plate" profile. From a structural pint of view, each of the volcanoes of the western Galapagos has a summit caldera with circumferential and radial eruptive fissures (Fig. 13.6a).

The circumferential fissures, rarely observed on active volcanoes elsewhere, are high and focused on the upper volcanic edifice, near the caldera rim. The radial fissures are scattered on the mid to lower slopes. This very distinctive fissure pattern results from the stresses due to the load of the volcanic edifice (for the radial fissures) and the unloading induced by the caldera depression (for the circumferential fissures; see Chap. 7; Chadwick and Howard 1991; Mouginis-Mark et al. 1996; Corbi et al. 2015).

The erupted magmas in the western Galapagos shield volcanoes are mainly tholeiitic, although alkali basalts may be locally present, as at Cerro Azul. Also, approximately 1 km^3 of rhyolite was erupted at Alcedo in the last 120 ka from at least three vents and in 2–5 episodes. These rhyolites result from fractional crystallization, which occurs because the volcano has been carried away from the hot spot. More generally, the variability of the magmatic systems of the western Galapagos volcanoes has been explained by their location with regard to the hot spot. At the leading edge of the hot spot, magmas are only partly buffered thermally and chemically (as at Cerro Azul). Once a volcano becomes mature (as Fernandina), magmas transit through a mush pile before residing in a shallow subcaldera sill, which buffers all magmas thermally and chemically and creates a monotonous suite: these volcanoes are the most active. In the dying

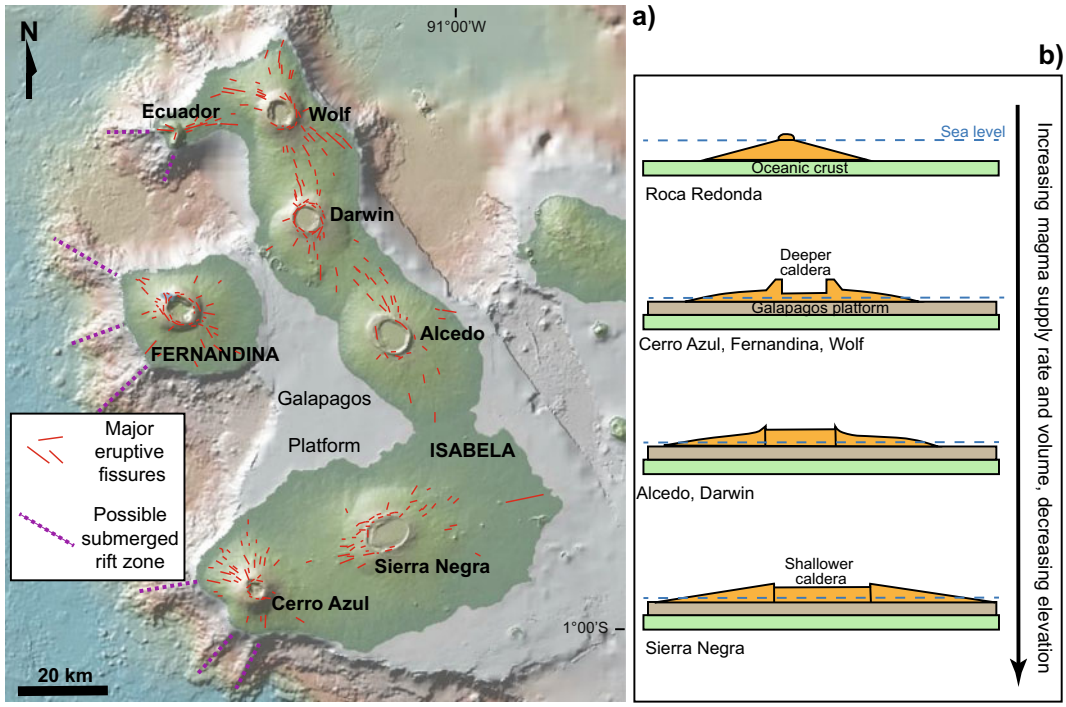

Fig. 13.6 Galapagos hot spot. **a** Overview of Fernandina and Isabela islands, western Galapagos, highlighting the calderas and the main eruptive fissures. Digital Elevation Model provided by GeoMapApp. **b** Model for the effect of magma supply rate on the growing forms of the western Galapagos shield volcanoes (orange, section view), from the lowest supply of the barely emergent conical volcano of Roca Redonda, to the highest supply of large shields (as Sierra Negra), with relatively shallow calderas and gently dipping flanks (modified after Naumann and Geist 2000)

phase, when the volcano is carried away from the hot spot, the mush begins to solidify and silicic magma is also generated (as at Alcedo). The lavas erupted from the eastern Galapagos are on the whole much more primitive (Geist et al. 2014; Harpp and Geist 2018, and references therein). Two discrete regions of magma storage have been often geodetically and petrologically inferred below some western (Wolf, Fernandina, Cerro Azul) and eastern Galapagos volcanoes. These regions consist of a shallower small magma lens and a major zone of magma storage in the lower crust, from which most of the erupted material is sourced (Stock et al. 2018).

Fernandina, ~30 km wide and ~1500 m high above sea level (a.s.l.), is the westernmost volcano, with a summit caldera, well-developed and focused circumferential fissures, and diffuse radial fissures. The caldera results from the last important collapse, reaching a maximum of 350 m in June 1968. A sill-like magma chamber and an oblate-spheroid cavity are postulated at 1.1 and ~4.9 km below sea level, respectively (Simkin and Howard 1970; Chadwick et al. 1991, 2011; Bagnardi and Amelung 2012). The eruptions from radial and circumferential fissures are usually fed by dikes initiated as sills from the shallow magma chamber. The sills propagate laterally, curve upward and steepen to become dikes when feeding circumferential fissures, or twist about a radially oriented axis to feed radial fissures on the volcano flanks (Fig. 7.8; Bagnardi et al. 2013).

Isabela is the largest island in the western Galapagos, resulting from the coalescence of six active volcanoes, each spaced by a few tens of kilometres and together encircling the eastern portion of Fernandina (Fig. 13.6a). From the

north, these are: Ecuador, Wolf, Darwin, Alcedo, Sierra Negra and Cerro Azul. Ecuador, at the northwest tip, provides two distinctive features. First, it experienced at least one sector collapse; this removed its western half of the edifice within the past 100 ka. Second, its eastern rift zone, which connects the volcano with Wolf, is constructed of lavas from focused and subparallel linear vents and shows evidence of a feeder conduit; this is the Galapagos structure that most closely resembles a Hawaiian rift zone (Rowland et al. 1994; Geist et al. 2002). The calderas of Alcedo and Sierra Negra volcanoes are both characterized by a minor trapdoor resurgence, with uplift of ~30 and ~100 m, respectively. Interestingly, their short-term asymmetric uplift, as geodetically observed in the last decades, has mimed the longer-term asymmetric resurgence (Chadwick et al. 2006; Galetto et al. 2019).

The observed variations in elevation, slope, volume and area among the western Galapagos volcanoes have been linked to different long-term eruption rates. Volcanoes with shallower calderas, as Sierra Negra, are constructed when radial fissures erupt voluminous lavas to produce a wide, flat shield with minimal, steep, upper flank segments. This behaviour may result from an intermediate to higher supply of magma in more mature volcanoes. Volcanoes with deeper calderas, as Fernandina, develop when numerous small-volume eruptions from circumferential fissures build a steep central summit carapace surmounting gently dipping lower flanks. This behaviour may result from a lower supply of magma in less mature volcanoes (Fig. 13.6b; Naumann and Geist 2000).

The central, northern and eastern Galapagos consist of several smaller islands with older record of activity, eroded inactive volcanoes or their remnants, and evidence of a regional structural control (Fig. 13.7). The northern volcanic province, including the islands of Genovesa and Pinta, results from the combination of excess temperatures, weak lithosphere and regional stresses developed from the interaction between the plume and the Galapagos Ridge. Genovesa formed in the past 350 ka, has ~NE-SW trending fissures parallel to the Genovesa Ridge, a 55 km long volcanic rift zone that is the most prominent submarine rift in the Galapagos, fed by the plume (Harpp et al. 2002, 2003). Pinta lies between Isabela and the Galapagos Ridge, 20 km to the west of the ~N-S trending Galapagos transform fault. It rises from a prominent

Fig. 13.7 Galapagos hot spot. Eroded neck (vertical spine to the right) and vents (in the foreground) accompanied by more recent monogenic volcanism (in the background) on the eastern coast of Santiago Island, central Galapagos

NNW-SSE trending submarine fault scarp, and its elongation reflects the control of this major structure. Regional NNW-SSE trending fracture systems also influenced the fissural volcanism postdating the shield volcano, which became emergent at ~0.7 Ma (Cullen and McBirney 1987). San Cristobal Island, at the eastern end of the archipelago, shows a central shield, formed until 0.6 Ma and, to the northeast, NE-SW trending fissure eruptions active from 0.9 Ma to historical times (Geist et al. 1986).

The differences between the western and the eastern Galapagos volcanoes, in terms of type of volcanic edifice, presence of calderas or rift zones, productivity and composition, have been related to the proximity to the wandering Galapagos Spreading Ridge (Harpp and Geist 2018). In particular, the magmatic flux of the volcanoes negatively correlates to the distance to the ridge: when the ridge was close to the plume, that is when the eastern Galapagos volcanoes formed, most of the plume-derived magma was directed to the ridge. Currently, the active western Galapagos volcanoes are farther from the ridge and most of the plume-derived magma focuses beneath the large young shields. The structure of the volcanoes seems also affected by the proximity to the ridge, with ridge-induced far-field stresses promoting linear volcanism with parallel rift zones in the eastern Galapagos, and plume-induced near-field stresses promoting central volcanoes with calderas and circumferential and radial rift zones in the western Galapagos. Therefore, rather than being controlled by plate motion across the hot spot, as with the Hawaiian volcanoes, the Galapagos volcanoes seem more affected by the changing far-field tectonic environment.

13.4 Easter Island Hot Spot

Easter Island (Chile) lies on the Nazca plate, ~350 km to the east of the East Pacific Rise bordering the Easter microplate, in the western part of the ~3000 km long Easter Seamount Chain. The Easter microplate formed approximately 5 Ma ago during the northward propagation of the eastern spreading segment of the East Pacific Rise and its overlap with the southward propagating western segment (Fig. 13.8a; Naar and Hey 1991; Searle et al. 1993; Rusby and Searle 1995).

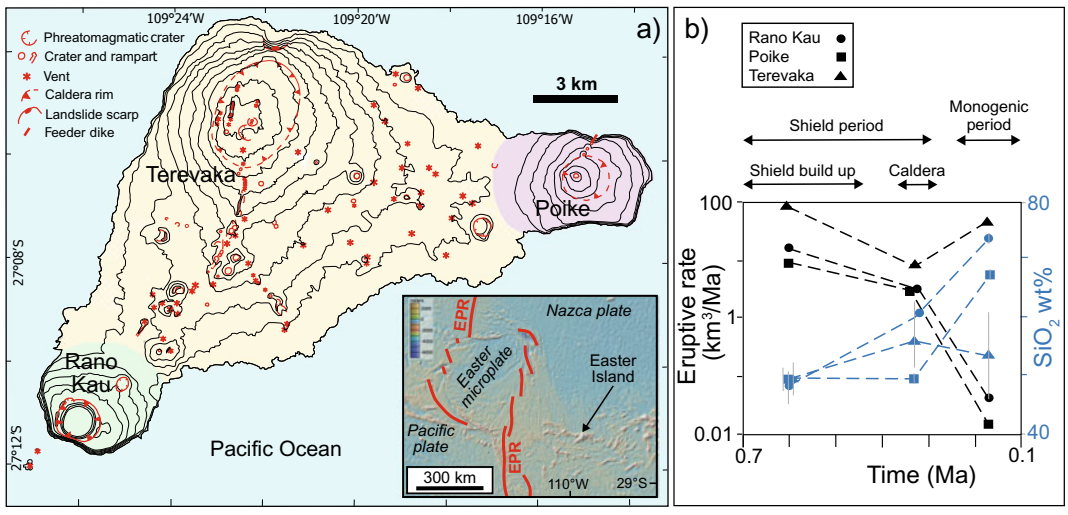

Fig. 13.8 Easter Island hot spot. **a** Structural map of Easter Island, Chile, showing the three volcanic edifices, the buried (dashed lines) and exposed (continuous lines) calderas and the eruptive fissures. Inset shows the regional setting, with the red lines representing segments of the East Pacific Rise. **b** Variation of the eruptive rates (in km^3/Ma, on a log scale; in black) and SiO_2 content of the lavas (in blue) with time considering the periods of shield build up, caldera formation and monogenic volcanism for each of the Easter Island volcanoes (modified from Vezzoli and Acocella 2009)

N-S trending ridges, parallel to the axis of the East Pacific Rise, characterize the oceanic floor of the ~350 km wide region between Easter Island and the East Pacific Rise. This region, characterized by 2–4 Ma old ocean seafloor, hosts several young (0.6–0.2 Ma) submarine volcanic seamounts. The age difference between the oceanic seafloor and its seamounts, as well as the volcanism younger than 0.78 Ma on Easter Island, indicates that the magmatism making up this western portion of the Easter Seamount Chain is intraplate (Naar and Hey 1991; Stoffers et al. 1994; Haase et al. 1997). More generally, radiometric dating along the Easter Seamount Chain shows progressively younger ages westward, confirming that the Easter Seamount Chain results from the motion of the Nazca plate over a mantle plume located immediately to the west of Easter Island and active for at least 30 Ma. Focal mechanisms from earthquakes in the area between Easter Island and the East Pacific Rise show predominant normal motion, with an overall NW–SE direction of extension (O'Connor et al. 1995; Haase 2002; Bird 2003; Ray et al. 2012).

Easter Island is the emerged portion, reaching ~500 m above sea level, of the submarine Rano Kau Ridge, rising for nearly 3000 m from the surrounding ocean floor. This ridge is ~NE-SW elongated, perpendicular to the extension direction revealed by the seismicity west of Easter Island. The emerged portion of Easter Island consists of three overlapping basaltic central volcanoes with a shield-like shape: Rano Kau, Terevaka, and Poike (Fig. 13.8a). Of these, Terevaka is the largest, with Rano Kau and Poike located on its southern and eastern slopes, respectively. These volcanoes range in composition from tholeiitic basalts to rhyolites, and the erupted lavas show considerable crystal fractionation, suggesting shallow magma chambers and a decreasing magma supply (Haase et al. 1997; Gonzalez-Ferran et al. 2004). The three polygenic volcanoes experienced a similar and nearly coeval evolution, characterized by two main stages (Vezzoli and Acocella 2009). The first stage, between ~0.78 and 0.3 Ma, consisted of the build up of the three basaltic shields (Fig. 13.9). This build up was associated with eruption rates of similar order of magnitude for the three volcanoes, although Terevaka grew faster. The SiO_2 content of the erupted magmas remained remarkably constant and low. The final part of the shield stage was characterized by caldera formation, with a significant drop (one order of magnitude) in the eruptive rates, as well as a slight increase in the SiO_2 content of the erupted magmas and the emission of more evolved highly porphyritic lavas (Fig. 13.8b). The second stage, between 0.24 and 0.11 Ma, was characterized by the activity of monogenic vents along the flanks of the three shields, with eruptive fissures showing a dominant NNE-SSW trend, subparallel to the ~NE-SW elongated Rano Kau Ridge. In addition to the preferred NNE-SSW orientation, part of the monogenic

Fig. 13.9 Panoramic view of Easter Island from the summit of Poike volcano, with the Terevaka and Rano Kau shield volcanoes and the post-shield monogenic volcanoes

vents on the Terevaka flanks also show an overall quite dispersed or scattered distribution, resembling poorly-developed or diffuse radial rift zones. During the monogenic stage, the supply to the magmatic systems of Poike and Rano Kau decreased, resulting in minor eruptions of silica-rich, highly viscous, residual and cooler magma. Conversely, the vents on Terevaka, associated with higher eruptive rates and lower SiO_2 content, suggest a more enriched mantle source, with input of new magma (Fig. 13.8b). The input of this new and more primitive magma prevented Terevaka reaching the evolved compositions of the other two volcanoes. The subaerial evolution of Easter Island thus appears controlled by the rise of moderate batches of magma in a context of decreasing supply. This decrease has been responsible for cooling the peripheral magmatic systems (Rano Kau and Poike volcanoes), allowing only the rise of magma through the larger Terevaka magmatic system and its eruption, mainly through radial dikes, along the volcano flanks. Another distinctive feature of Easter Island is the very limited evidence of flank instability and collapse, possibly restricted to a minor northern portion of the Terevaka shield (Vezzoli and Acocella 2009).

Because of its tectono-magmatic features and limited activity, testified by a low eruptive rate, generally diffuse rift zones and very limited lateral collapse, Easter Island may represent an end-member type of oceanic hot spot volcano, opposite to Hawaii.

13.5 Reunion Hot Spot

The Reunion hot spot lies on the African plate, in the southwest Indian Ocean. The products of the 5000 km long ~N-S trending hot spot track highlight a homogeneous, compositionally primitive plume source and include the Deccan basalts (68–66 Ma) and the submarine ridge below the Maldives (55–50 Ma). The most recent hot spot activity has produced the southern Mascarene Ridge, which includes the islands of Mauritius (8.9–0.03 Ma), to the northeast, and Reunion (2.1–0 Ma), to the southwest (Fig. 13.10; Bonneville et al. 1997; O'Neill et al. 2003).

While the present plume conduit, with radius of 100–130 km and upwelling velocity of 5–9 cm/year, lies at an asthenospheric depth at 100–200 km north of Reunion, the hot spot is centred beneath Piton de la Fournaise volcano, in the eastern portion of Reunion Island. The plume may not consist of a single body, as the composition of the Reunion lavas may result from the impingement of two small-scale blobs of plume at the base of the lithosphere (Barruol and Fontaine 2013). A partially molten layer lies at the crust-mantle boundary beneath Reunion. This underplated body is 140 km wide and up to 3 km thick. The oceanic plate around Reunion is not flexurally downwarped toward the island, but instead domed toward southeast. The historical effusive rate of Reunion of $\sim 10^4$ km^3/Ma suggests that its submarine growth began 5–7 Ma ago. Most of the volume edifice is submerged: the volcanic edifice appears as a flattened cone 200–240 km wide, whose subaerial part is only 3% in volume, and whose history spans only the last 2.1 Ma (Charvis et al. 1999; Gallart et al. 1999). Reunion results from at least three volcanic complexes. An inferred older volcano, Les Alizés, below the eastern coast has a large intrusive and cumulate complex, at 1 km depth (Gailler and Lenat 2012). Most of Reunion is constituted by the larger and older Piton des Neiges volcano, to the northwest, and the more recent Piton de la Fournaise volcano, to the southeast, active simultaneously for more than 500 ka (Fig. 13.10). The location and direction of the alignment of both volcanoes and of their connecting rift zone are consistent with an inferred NW–SE trending pre-existing regional structure, whose reactivation may result from the uplift related to the strong underplating (Michon et al. 2007). The magmas erupted at Piton des Neiges and Piton de la Fournaise are mostly olivine basalts, with a composition transitional between tholeiitic and alkali basalts, although progressively evolving towards increasing tholeiitic compositions (Albarede et al. 1997).

Piton des Neiges is a dormant volcano at least 2.08 Ma old. Following a basaltic shield stage

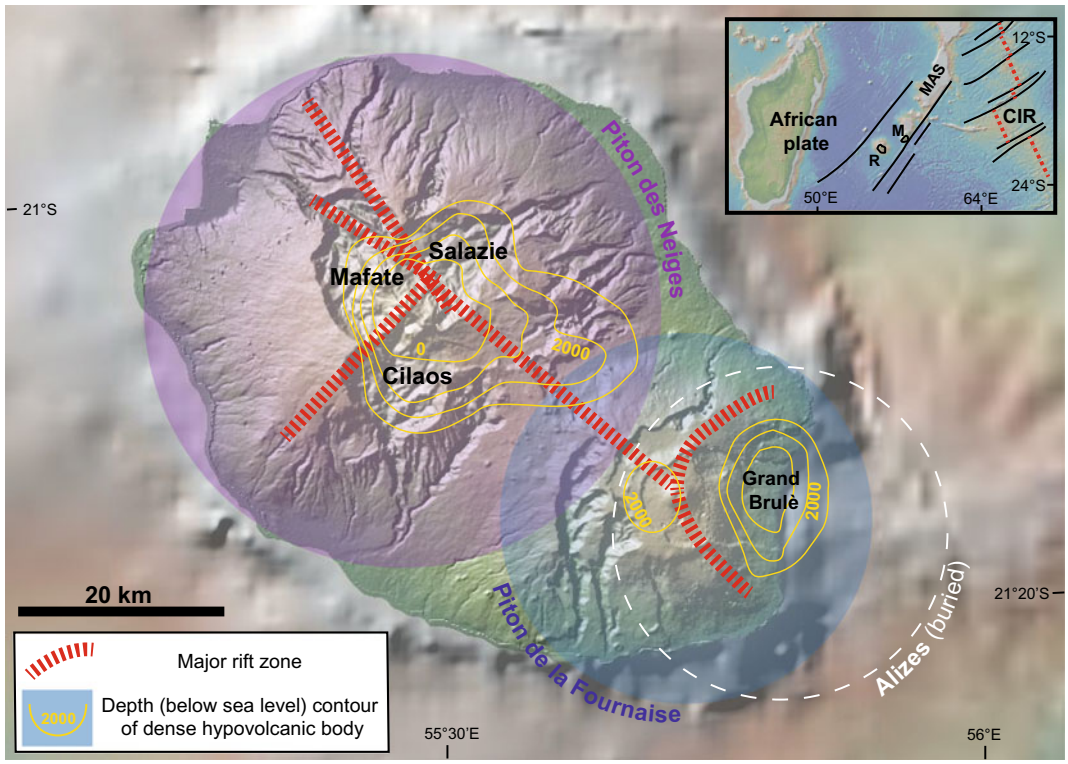

Fig. 13.10 Overview of the island of La Reunion, Indian Ocean, highlighting its three main volcanic edifices, the major volcanic rift zones and the depth contours (in metres below sea level) of buried dense intrusions (from Michon et al 2007; Gailler and Lenat 2012). Inset shows the tectonic setting of the hot spot, along the Mascarene Ridge (MAS); R = Reunion Island; M = Mauritius Island; CIR = Central Indian Ridge. Digital Elevation Models provided by GeoMapApp

(2.08 to 0.43 Ma), it erupted alkaline differentiated lavas (350–12 ka). The volcano is deeply eroded within three main depressions: the Mafate, Salazie and Cilaos Cirques (Fig. 13.10). Minimum eroded volumes of 101 and 105 km^3 have been calculated for the last 180 ka for the Mafate and Cilaos depressions, respectively, giving a minimum long-term erosion rate of 1.2 km^3/ka. The products of the erosion are found on the ocean floor, in large fan-shaped promontories 20–25 km wide at the coastline and 70–150 km across the seafloor. These result from the superimposition of multiple debris avalanche deposits. A hydrothermally altered intrusive complex beneath Piton des Neiges is deeply rooted, to several kilometres below sea level, and is 10–25 km wide (Lenat et al. 2001; Oehler et al. 2004; Gailler and Lenat 2012). Above, three perpendicular intrusion trends (two subvertical and one subhorizontal) coexisted for 2 Ma. Stress accumulation under repeated magma injections resulted in permutations of the principal axes of the stress tensor, reorienting subsequent intrusions. Intrusions cycles started with dike injections in an extensional stress field, reducing the deviatoric stress, then switching the axes of principal stresses and finishing with sill intrusions in a compressional stress field. Sills acted as detachment planes, restoring the extensional stress field and initiating a new cycle of permutations (Chaput et al. 2014).

Piton de la Fournaise has two building stages, described as the Ancient (0.53–0.15 Ma) and Recent Shields (<0.15 Ma). These were separated by a collapse event that shifted the volcano centre eastward by about ~15 km, from the

present-day Plaine des Sables to the current position of the active summit. Two main subvolcanic intrusions are the Grand Brûlé complex, below the Grand Brûlé depression on the easternmost flank of the volcano, and a complex beneath the Plaine des Sables and the Enclos Fouqué, on the western part of the volcano. The Grand Brûlé complex, N-S elongated and deeply rooted, is the relict of the Alize's Volcano. The subcircular Plaine des Sables-Enclos Fouqué complex was the center of the Ancient Shield before the collapse event, and currently hosts a large and active hydrothermal system (Gailler and Lenat 2012; Dumont et al. 2019). Four U-shaped structures opening seaward are nested on Piton de la Fournaise (Fig. 13.11). The innermost and youngest collapse is the 13 km long and 6–8 km wide Enclos Fouqué-Grand Brûlé depression, E-W elongated and delimited by a horseshoe rim to the west, south and north sides with a continuous cliff, 100–200 m high (Staudacher and Allegre 1993; Gillot et al. 1994; Merle et al. 2010a).

Several hypotheses have been proposed to explain the origin of the Enclos Fouqué-Grand Brûlé depression (Fig. 13.12). A first model suggests that the Enclos Fouqué-Grand Brûlé results from a 4.5 ka old giant landslide partly responsible for the debris avalanche deposits on the submarine flanks (Gillot et al. 1994). A second model suggests that the entire Enclos Fouqué-Grand Brûlé results from vertical collapse, due to the deformation of the hydrothermal system and the downward drag related to the dense intrusive complex of the underlying Alize's volcano (Michon and Saint-Ange 2008). A third set of models suggests that the Enclos depression results from a polyphase caldera collapse, whereas the Grand Brûlé exhibits the scars of lateral landslides with the headwall immediately to the east of the caldera. In this model, the clay-rich altered and pressurized hydrothermal core of the volcano may flow under its own weight, spreading laterally in the Grand Brûlé area and triggering caldera-like collapse in the summit area (Merle and Lenat 2003; Merle et al. 2010b).

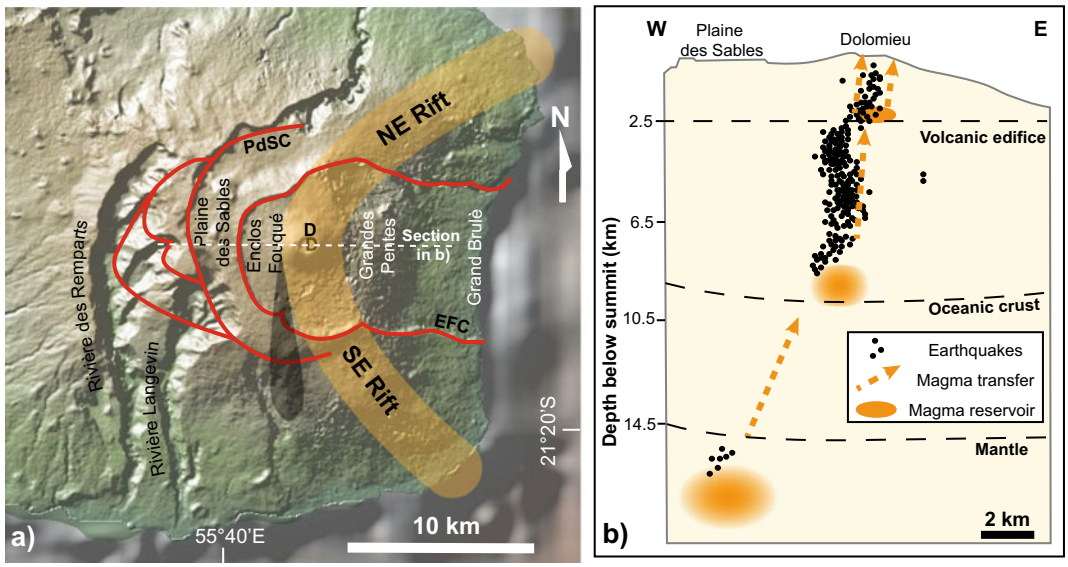

Fig. 13.11 La Reunion hot spot. **a** Simplified structural map of Piton de la Fournaise volcano, including the main rift zones (in orange) and structures (in red); PdSC = Plaine del Sables collapse; EFC = Enclos Fouqué-Grand Brûlé collapse; D = Dolomieu caldera (Merle et al. 2010a; Bonali et al. 2011). Digital Elevation Model provided by GeoMapApp. **b** East–west cross section through Piton de La Fournaise, showing the location of the 1996–2007 earthquakes and magma storage at depth (modified after Peltier et al. 2009)

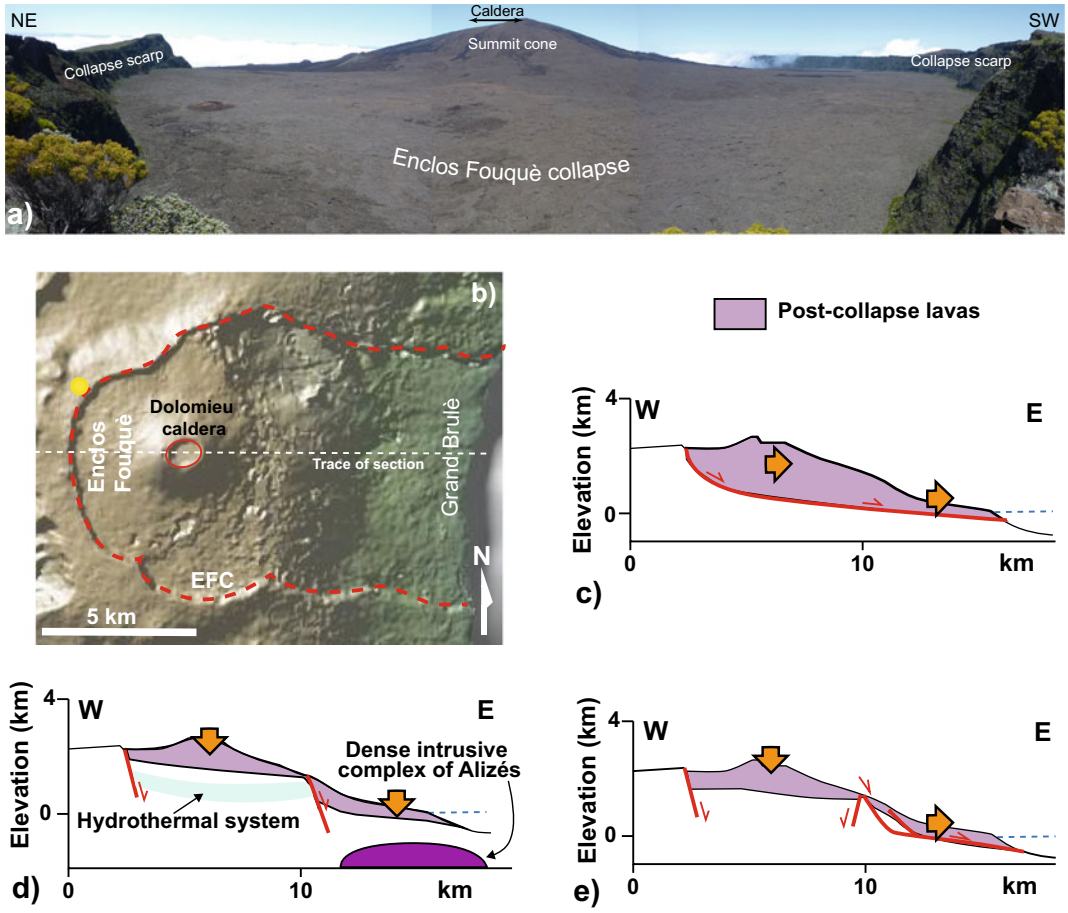

Fig. 13.12 La Reunion hot spot. **a** View from the northwest part of the Enclos Fouquè collapse scarp towards the Dolomieu cone, Piton de la Fournaise volcano. **b** Schematic map view of Piton de la Fournaise and the Enclos Fouqué-Grand Brûlé collapse (yellow dot shows point of view in (**a**). **c**–**e** Schematic end-member models (in E-W cross section) proposed for the formation of the Enclos Fouqué-Grand Brûlé structure: **c** a single landslide (lateral collapse); **d** a vertical collapse, due to the deformation of the hydrothermal system and the downward drag related to the dense intrusive complex of the underlying Alize's volcano; **e** a polyphase caldera collapse, where the Grand Brûlé is the scar of one or several lateral landslides (Michon and Saint-Ange 2008). DEM in (**a**) provided by GeoMapApp

The Enclos Fouqué-Grand Brûlé depression shares close similarities with the U-shaped collapse structures observed on other hot spot oceanic islands, as at Tenerife (Las Canadas caldera; see Sect. 13.6) and Fogo (Cape Verde). At Fogo, the U-shaped scarp affecting the summit and side of the volcano has been interpreted as a caldera or part of lateral collapse (Fig. 6.1e; Day et al. 1999, and references therein; Masson et al. 2008).

Piton de la Fournaise is a highly active shield, with an average of one eruption every 10 months over the last decades. Present-day summit activity focuses in a 400 m high basaltic cone with caldera (Dolomieu) and pit crater (Bory). Dolomieu caldera has developed by sudden collapses above a 1.5 km wide high velocity plug located above sea level, corresponding to an intrusive, solidified dike and sill complex. Below, two low velocity anomalies, from 1 to 0 km a.s.l. and

deeper than 1 km below sea level, correspond to magma storage systems. Dolomieu experienced its last caldera collapse in 2007. To the sides of Dolomieu are the northeast and southeast rift zones, which are among the most developed of the six rift zones of the volcano. These rift zones lack a pronounced topographic expression, as mantling pre-existing topography, and are relatively diffuse (Fig. 13.11; Lenat et al. 1989; Michon et al. 2009; Prono et al. 2009; Bonali et al. 2011).

13.6 Canary Islands Hot Spot

The Canary Islands lie on Jurassic oceanic lithosphere near the west African continental margin. The archipelago consists of seven major islands with east-to-west age progression of ~1.9 cm/year, starting from the oldest subaerial volcanism at ~20 Ma for the eastern islands of Lanzarote and Fuerteventura, to ~15 Ma for Gran Canaria, 8 Ma for Tenerife and less than 2 Ma for the western islands of La Palma and El Hierro (Fig. 13.13).

This progression is compatible with the slow passage of the African plate over a hot spot, currently located beneath the western part of the archipelago. Some features may be difficult to reconcile with a typical hot spot, such as the low melting rate, the tens of Ma long volcanic history at single volcanic centres with long gaps, and the irregular distribution of volcanism. These features suggest that other processes, such as lithospheric intraplate deformation, accompany plume volcanism (Carracedo et al. 1998; Danobeitia and Canales 2000; Geldmacher et al. 2005).

The isotopic signature of the Canary Islands magmas, intermediate between that of the Madeira hot spot to the north and the Cape Verde Islands hot spot to the south, suggests a common, large-scale mantle upwelling off west Africa (Abratis et al. 2002). A low velocity layer, with less than 3% melt, lies at 45–65 km of depth within the thinned lithosphere of the Canary Islands. The Moho deepens eastward, from ~12 to ~25 km. A regional anomaly of ~500 m above the thinned lithosphere, probably related to a sub-lithospheric temperature anomaly of +100 °C, produces a topographic swell partly

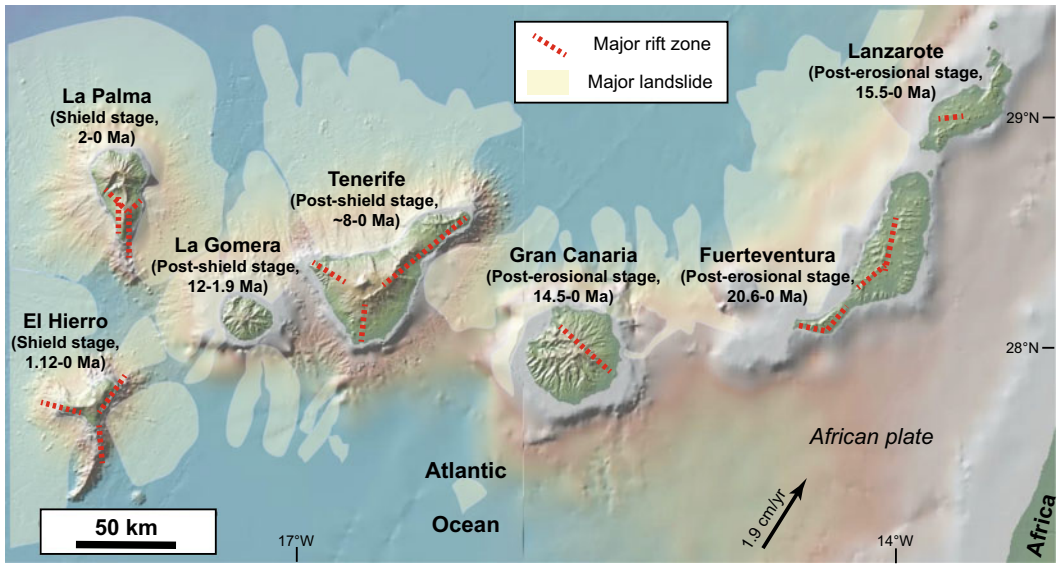

Fig. 13.13 Overview of the Canary Archipelago, highlighting the ages and evolutionary stage of the islands, their main rift zones and submarine landslides; plate velocity is with regard to the hot spot (Carracedo 1999). Digital Elevation Model provided by GeoMapApp

masked by thick sediments and the volcanics of the Canary Islands. Superimposed on this swell is a flexural moat that flanks the Canary Islands, induced by the load of the volcanoes (Collier and Watts 2001; Martinez Arevalo et al. 2013; Fullea et al. 2015). Underplating and crustal thickening by mafic intrusions, usually ranging from 2 to 8 km, occurs along the Moho and the base of the elastic lithosphere beneath Gran Canaria, La Palma, Tenerife, Fuerteventura and Lanzarote. Low velocity zones beneath La Palma and Tenerife are interpreted as due to partial melting (Danobeitia and Canales 2000; Lodge et al. 2012).

Individual islands show initial rapid growth (shield-building stage), followed by quiescence, deep erosion and post-erosional activity. The western islands, La Palma and El Hierro, are the youngest and still in their shield stage. Volcanic activity occurs in these islands and persists in Tenerife and Lanzarote. The composition of the volcanic rocks of the Canary Islands is highly variable, ranging from mafic (transitional tholeiite to melilite nephelinite) to highly evolved (peralkaline rhyolite to trachyte to phonolite). While alkali basalts and tholeiites are the dominant shield-building magma types, highly differentiated magmas, as quartz-trachytes and phonolites, develop mainly during the waning stages (Hoernle and Carracedo 2009).

The Canary shields contain volcanic rift zones, which are best displayed on the younger volcanoes, such as La Palma, El Hierro and Tenerife. These rift zones, each several tens of kilometres long, are usually arranged in three arms, where angles between each rift ideally are 120° (Fig. 13.13). The rift zones range from linear ridges to broad fans at the base of the volcanic edifice. The fanning may reflect: (a) non suitable stress field for trapping dikes within the rift, (b) dike injection migrating laterally, (c) stress field interactions between volcanic edifices, and (d) low rate of magma supply for dike propagation (Carracedo et al. 1998; Acosta et al. 2003). While the concept of three-arm rifts has been accepted for decades as a distinctive feature of the Canary Islands volcanoes, recent studies suggest that these rifts rather result from initial radial eruptive fissures that have been obscured by successive flank collapses (Becerril et al. 2015). The growth of rift zones includes the oversteepening, the instability and the lateral collapse of the flanks to the sides, with dike-induced rifting appearing as the main trigger for flank destabilization and ultimately dismantling the islands. At the shield-stage islands, several Quaternary debris avalanches extend tens of kilometres offshore (Fig. 13.13). There is a higher landslide frequency for the Canary Islands compared to the Hawaiian Islands. The lower stability of the flanks of the Canary Islands may be due to their steeper slopes, a result of the abundance of highly evolved viscous lavas, and the abundance of weak pyroclastic deposits deriving from frequent explosive eruptions due to the elevated volatile contents in the alkalic magmas (Carracedo 1999; Krastel et al. 2001).

The main tectono-magmatic features of some representative islands, from east to west, are summarized below.

Fuerteventura, the oldest island, is distinctive for its long and discontinuous volcanic history, interspersed with major erosional phases. Fuerteventura began and ended its shield stage in the Miocene. The shield was truncated by giant landslides by 17.5 Ma, which removed 3500 km^3 of volcanic material and stripped the volcano down to the pre-shield phase of the Basal Complex. The latter represents the submarine growing stage of the volcanic complexes and the hypabyssal roots (plutons and dikes) of their successive subaerial growing episodes, subsequently affected by long-lived Miocene tectonic activity. After the shield stage an extended period of quiescence and erosion was followed by minor Pliocene and Quaternary post-erosional volcanism (Ancochea et al. 1996; Stillmann 1999; Fernandez et al. 2006).

Tenerife is the product of complex and diversified volcanic activity. The island results from the coalescence of three shields: Roque del Conde to the southwest (between 11.9 and 8.9 Ma), Teno to the northwest (6.2–5.6 Ma) and Anaga to the northeast (4.9–3.9 Ma) (Fig. 13.14). These shields formed the bulk of subaerial Tenerife since 8 ± 4 Ma, with each

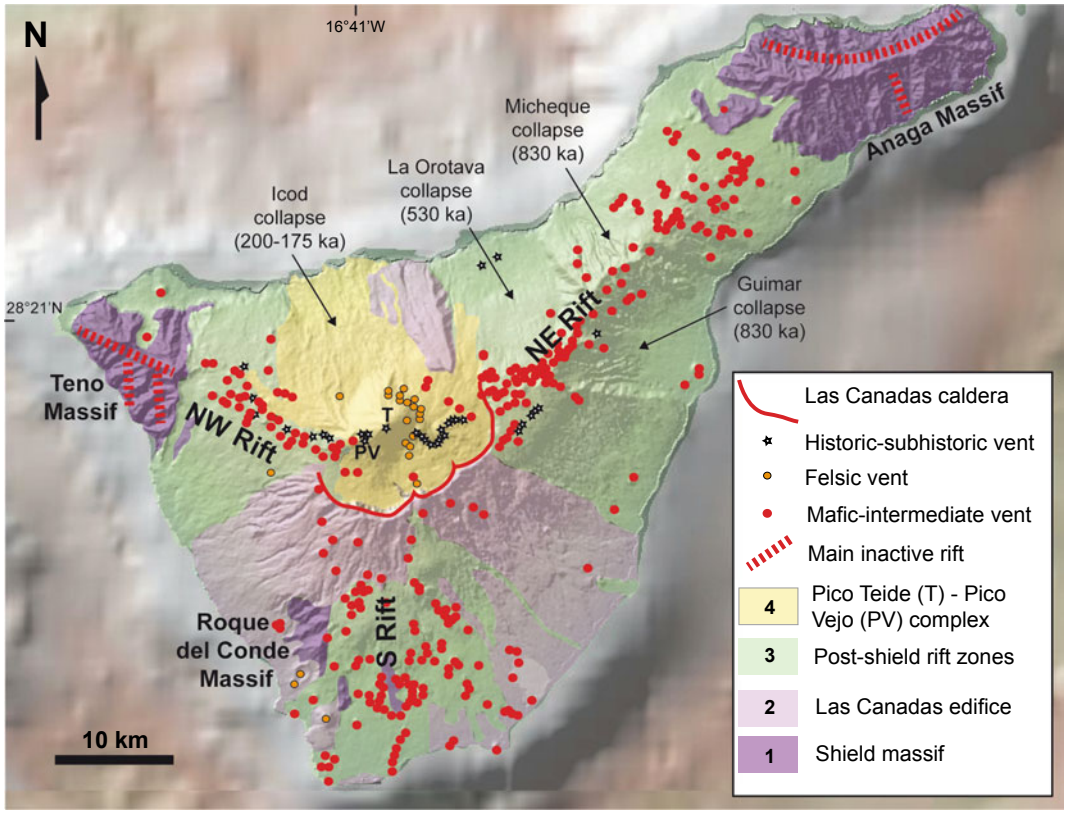

Fig. 13.14 Canary Islands hot spot. Structural map of Tenerife, highlighting the older massifs, the rift zones, the summit caldera and the lateral collapse scarps (modified after Martì et al. 2009)

shield constructed in less than 3 Ma (Guillou et al. 2004). The Anaga basaltic shield volcano was initially dominated by a single rift zone. Destabilization of the northern sector resulted in a collapse and the bending of the rift. Induced by the dilatation of the curved rift, a third rift-arm developed to the south, generating a three-armed rift system (Fig. 6.9; Walter et al. 2005). After the coalescence of the three volcanoes, a significant part of the Tenerife shield was removed by repeated giant landslides. The shield-building stage was thus followed by 2–3 Ma of erosion and volcanic quiescence. Eruptions resumed during the stage of rejuvenation, when the central volcano of Las Cañadas, 40 km wide and ~3000 m high, developed unconformably over the Miocene shield (Fig. 13.14). The central volcano developed three main rift arms (to the south, northwest and northeast), with major collapses in between (Carracedo et al. 2007; Boulesteix et al. 2013). The Las Cañadas volcano summit also collapsed between 200 and 175 ka, creating the Las Cañadas depression (Fig. 13.15). This is explained as the head of a gravitational collapse or, more likely, as the coalescence of three successive caldera collapses due to the emptying of a migrating magma chamber following large eruptions. The twin volcanoes of Pico Teide and Pico Viejo developed within the caldera, marking the most recent eruptive cycle (Martì 2019, and references therein). The oceanic basement dips gently towards the island, whose load forms a flexural moat filled by 2–3 km of sediments. Up to 1.5×10^5 km^3 of magmatic material has been added to the flexured oceanic crust, with magma

Fig. 13.15 Tenerife, Canary Islands: view of the central portion of Las Cañadas caldera (foreground), as seen from the south rim, with Pico Teide on the background

generation rate of 10^3–10^4 km^3/Ma, similar to Reunion and Cape Verde, but at least an order of magnitude less than Hawaii (Watts et al. 1997).

El Hierro is the youngest and westernmost island. The oldest subaerial part is 1.2 Ma old. Eruptive activity has been nearly continuous, growing two successive edifices affected by one or more catastrophic lateral collapses: Tinor (1.2–0.88 Ma) and El Golfo (545–176 ka). After 158 ka, volcanic activity was fed from the present-day rift zones, arranged in the three-armed configuration (Fig. 9.2; Day et al. 1997). Overgrowth instability due to successive rift eruptions has led to several flank failures and giant landslides, the last of which occurred to the north between 130 and 100 ka, resulting in the trilobed shape of the island. The San Andres fault system identifies, along the eastern flank of the northeast rift zone, the failure zone of a giant landslide which has slipped twice between 540 and 430 ka and between 183 and 52 ka (Day et al. 1997; Blahut et al. 2020). Data offshore El Hierro suggest that rifting is not confined to narrow zones. The young Las Hijas volcanic seamounts, 70 km southeast of El Hierro, are consistent with the spacing and timing of propagation of volcanism of the archipelago, and these seamounts may represent future sites of volcanic islands. The last eruption occurred offshore south of the island in 2011 (see Sect. 9.2).

13.7 Azores Hot Spot

Although located next to the Mid-Atlantic Ridge, the Azores Archipelago shows a structure that is mainly controlled by the transtensive motion along the transform plate boundary between the Eurasian and African plates, to the east of the Ridge. This far-field influence motivates the inclusion of the Azores hot spot in this chapter, rather than in Chap. 11, which illustrates the

tectono-magmatic features of divergent plate boundaries and includes the Afar and Icelandic hot spots. In particular, the Azores Archipelago straddles the Mid-Atlantic Ridge in the area of a triple junction that includes an oblique and recently formed ultraslow rift, a zone of diffuse seafloor deformation, a major fracture zone and a hot spot (Fig. 13.16).

The archipelago is mostly developed to the east of the Mid-Atlantic Ridge, with only two islands to the west of it. A low velocity anomaly in the shallow mantle (<200 km deep) is imaged under the central group of islands, to the east of the ridge. The low velocity anomaly extends northeastward and downward to connect to a column of low velocity material from ~250 km to at least 400 km of depth. The mantle upwelling velocity is estimated at 3–4 cm/year, smaller than that of Hawaii or Iceland (Yang et al. 2006; Madureira et al. 2014). Plume-ridge interactions and underplating between ~20 and ~7 Ma produced a submarine plateau, on which the Azores Islands lie, shallower than 2000 m, related to a 12–14 km thick crust, thicker than average. The plateau records episodic variations of the hot spot melt production with cyclicity of 3–5 Ma and, following a decrease in the rate of volcanism, it has been rifted by the Mid-Atlantic Ridge since 7 Ma (Gente et al. 2003; Spieker et al. 2018).

The main structures in the Azores area are the Mid-Atlantic Ridge, the Terceira Rift and the East Azores Fracture Zone (Fig. 13.16). The Mid-Atlantic Ridge separates the Eurasian and African plates from the North American plate. The structure and kinematics of the Eurasian-African boundary appears complex. Geodetically, Santa Maria Island, to the southeast, has been following the average African plate movement and Graciosa Island, to the north, has mimicked the average Eurasian plate behaviour, while the other islands display intermediate behaviours. Seismo-tectonic studies locate the main plate boundary between Sao Jorge and Pico, continuing to the east south of Sao Miguel. Other studies suggest that the main plate boundary is the 550 km long ultraslow Terceira Rift, which corresponds to a WNW-ESE trending alignment of segmented and alternating basins and volcanic edifices (Searle 1980; Madeira and

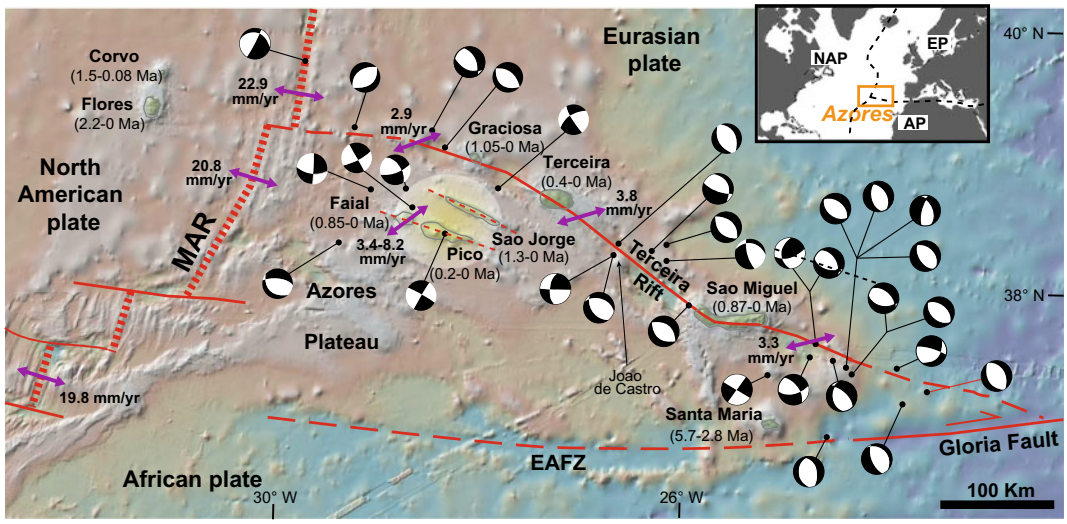

Fig. 13.16 Main features of the Azores Archipelago, including the ages of the islands, the main fault zones (solid and dashed thin red lines) and related opening directions (purple double arrows), and the focal mechanisms of the 1939–2013 M > 5.0 earthquakes. Inset shows the general tectonic setting. Light yellow circle = shallow hot spot location, from –75 to –188 km; MAR = Mid-Atlantic Ridge; EAFZ = East Azores Fracture Zone; NAP = North American plate, EP = European plate; AP = African plate (modified after Trippanera et al. 2014). Digital Elevation Model provided by GeoMapApp

Ribeiro 1990; Vogt and Jung 2004; Fernandes et al. 2006). The Terceira Rift formed ~1 Ma ago and is currently obliquely slowly spreading at 0.2–0.4 cm/year, with WSW-ENE trending extension and dextral component of motion (Fig. 13.16; Pagarete et al. 1998). This motion may result from the different spreading rate of the Mid Atlantic Ridge north (~2.3 cm/year) and south (~1.9 cm/year) of the Azores and the related overall lateral motion between the Eurasian and African plates of ~0.4 cm/year. Four volcanic systems (Sao Miguel, Joao de Castro, Terceira and Graciosa, three of which are islands) along the Terceira Rift are separated by deep non-volcanic basins, similar to ultraslow ridges (see Sect. 11.4.1). The interaction of obliquity, slow spreading rates and thick lithosphere probably prevents larger amounts of melt from reaching the surface. East of the Terceira Rift, the Eurasian-African plate boundary lies along the Gloria Fault, an E-W trending right-lateral transform fault moving at ~0.5 cm/year and reaching Gibraltar (Fig. 13.16; Searle 1980; Vogt and Jung 2004; DeMets et al. 2010). The East Azores Fracture Zone is the westernmost continuation of the Gloria Fault towards the Mid-Atlantic Ridge, to the south of the Terceira Rift. It corresponds to an aseismic and non-volcanic fault system, probably an Eurasian-African boundary abandoned after the northward migration of the triple junction. Therefore, the transtensive Azores region acts simultaneously as ultraslow rift and transfer zone between the Mid-Atlantic Ridge and the Gloria Fault, accommodating the differential shear between the Eurasian and African plates (Lourenço et al. 1998; Vogt and Jung 2004). The Mid-Atlantic Ridge spreading rates do not change abruptly in the area of the Azores triple junction. Rather, they change gradually, suggesting that the Mid-Atlantic Ridge, the Terceira Rift and the East Azores Fracture Zone constitute the boundaries of the kinematically distinct Azores domain, possibly a microplate, with distributed deformation and semi-rigid behaviour (Madeira and Ribeiro 1990; DeMets et al. 2010; Marques et al. 2013).

Seismicity focuses along the Terceira Rift and close to the Faial-Pico Fracture Zone and the Gloria Fault (Fig. 13.16). Focal mechanisms from 1939 to 2013 highlight predominant ~NW–SE oriented normal faults, extending along a NE-SW direction, and minor ~WNW-ESE trending dextral faults and ~NW–SE to NNW-SSE trending sinistral faults. While strike-slip motions predominate in the western portion, the eastern portion undergoes predominant extension, with average slip rate of 0.4 cm/year. Overall, there is a transtensive setting with partition between strike-slip and extensional structures. The estimated magnitudes of the largest paleoearthquakes range from *M6.9* to *M7.1*. Paleoseismological slip rates of 0.1–0.4 cm/year from Faial, Pico and Sao Jorge validate longer-term rates (Lourenço et al. 1998; Madeira and Brum da Silveira 2003; Trippanera et al. 2014). Several sets of faults, with N120 °E, N150 °E and ~N-S directions, define crustal blocks accommodating the interaction between the three main plates. Directions from N110° to N125°, focusing along the Terceira Rift, are interpreted as ancient fracture zones reactivated as transtensional faults. N-S directions are interpreted as former mid-oceanic rift faults reactivated as left-lateral faults (Navarro et al. 2009).

As a result of the activity of the transtensive plate boundary, several of the Azores volcanoes show distinctive morphological, structural and volcanological features. In fact, at least three islands appear strongly elongated (Sao Miguel, Sao Jorge and Pico) parallel to the plate boundary. The elongation is highlighted by transtensive fault systems, fissure eruptions forming focused rift zones and aligned polygenic and monogenic volcanoes. In some cases, as for example at Pico (see Fig. 7.22b), the rift zones extend outside the polygenic volcanoes for tens of kilometres, highlighting strongly elongated zones of magmatic activity, resembling magmatic systems along divergent plate boundaries (see Chap. 11). The development of long and focused rift zones is only partly associated with flank instability, which appears relatively limited on the Azores. In fact, despite frequent recognition of unstable and collapsed volcanoes flanks, as at Pico and Sao Miguel, only a few of the Azores islands show widespread mass-wasting processes

affecting their growth, as Flores and Santa Maria (Hildenbrand et al. 2012, 2018; Costa et al. 2014; Sibrant et al. 2015; Marques et al. 2020). Several volcanoes currently host calderas, as Sao Miguel, Terceira, Faial and Corvo, whose formation is usually associated with the emission of more evolved magmas. The magmas erupted in the Azores belong to an alkaline series, exhibiting the full range of compositions, from mafic to felsic. Generally, while the polygenic volcanoes erupt alkali basaltic to trachytic magma, the monogenic volcanoes from the fissure zones erupt basalts and hawaiites; rhyolites have been erupted at the Santa Barbara polygenic volcano, on Terceira Island (Larrea et al. 2018, and references therein).

The tectono-magmatic features of some representative Islands, from east to west, are summarized below.

Sao Miguel, along the eastern Terceira Rift, is the largest island, E-W elongated. Geodetic data suggest that any inferred plate boundary deformation zone at Sao Miguel is narrow, with 75% of the 0.4–0.5 cm/year full plate motion being accommodated over the 10 km width of the island. Sao Miguel consists of six Quaternary loci, which include calderas (Sete Cidades, Agua de Pau and Furnas), stratovolcanoes, shield volcanoes affected by flank collapse and elongated monogenic fields (Moore 1990; Trota et al. 2006; Sibrant et al. 2015).

Sao Jorge, despite its strong WNW–ESE elongation suggesting a far-field tectonic control, is moving neither with Eurasia nor with Africa, presenting two sectors with different behaviour: the northwest sector moves at 0.2 cm/year to N82 °E, while the southeast sector moves at 0.1 cm/year to N109 °E. This velocity field, not explained by slip along the active faults of the island, may be induced by local shallow magmatic processes (Mendes et al. 2013). Horizontal or sub-horizontal flow predominates within the dikes outcropping at Sao Jorge, suggesting that the ascent of magma occurs mainly over localized melting sources, then collected within shallow magma chambers and from here laterally delivered along the island (Silva et al. 2012; Moreira et al. 2015).

Pico and Faial are two nearby WNW-ESE elongated islands with collinear configuration located above the plume head.

Pico, to the east, is the youngest island of the Azores, dominated on its western sector by the stratovolcano of Pico Mountain, active from 57 ka at least, rising $\sim$2.5 km a.s.l. (Fig. 13.17). Several eruptions produced cones and fissures on its western and southeast flanks (Fig. 7.22b). Other major volcanic complexes on Pico include basaltic shield volcanoes (Topo volcano) and monogenic volcanic ridges (the Achada Plateau). Two major collapses affect the northern flank of Pico, where a main debris field larger than

Fig. 13.17 Azores hot spot. The imposing summit of Pico Volcano on the Island of Pico seen from Faial, with the Pedro Miguel Graben in the foreground bordered by two sets of oppositely dipping faults, highlighted by the white (outer fault systems) and yellow (inner fault systems) triangles

10 km^3 and with minimum age of ~70 ka is observed offshore (Nunes et al. 2006; Costa et al. 2014).

Faial, to the west, consists of four main and distinctive units (Fig. 13.18). The oldest volcanic system, to the east, was mainly built around 850 ka, then faulted to form the WNW-ESE-trending Pedro Miguel Graben (Fig. 13.17). An elongated high density body below and parallel to the axis of the Pedro Miguel Graben, interpreted as a solidified dike swarm, suggests that part of the graben is dike-induced. The Caldeira Central Volcano (~130 ka to Present) partly developed within the Pedro Miguel Graben with a summit caldera mainly formed at ~1 ka; a low Vp anomaly at 3–7 km depth images a magma chamber below. The youngest part of the island is the Capelo Peninsula fissure system, west of Caldeira. This consists of a basaltic ridge formed by WNW-ESE aligned vents. Capelo fed the two historical eruptions on Faial: the Cabeço do Fogo eruption in 1672–73 and the Capelinhos Surtseyan eruption in 1957–58 (Romer et al. 2018). The NE-SW trending mean extension rate of the Pedro Miguel Graben has been of 0.3–0.8 cm/year, similar or slightly larger than that of the Terceira Rift. This suggests that Faial, with the nearby Pico Island, where the graben continues buried by recent volcanic deposits, is a major locus of extension within the Azores above the imaged hot spot. The Faial-Pico tectonic segment may thus constitute the offset, westward continuation of magmatic activity to the southwest of the Terceira Rift, or one of the several major structures making up the presently diffuse plate boundary (Madeira and Brum da Silveira 2003; Camacho et al. 2007; Marques et al. 2013; Trippanera et al. 2014).

Flores and Corvo lie west of the Mid-Atlantic Ridge and are both derived from the same mantle

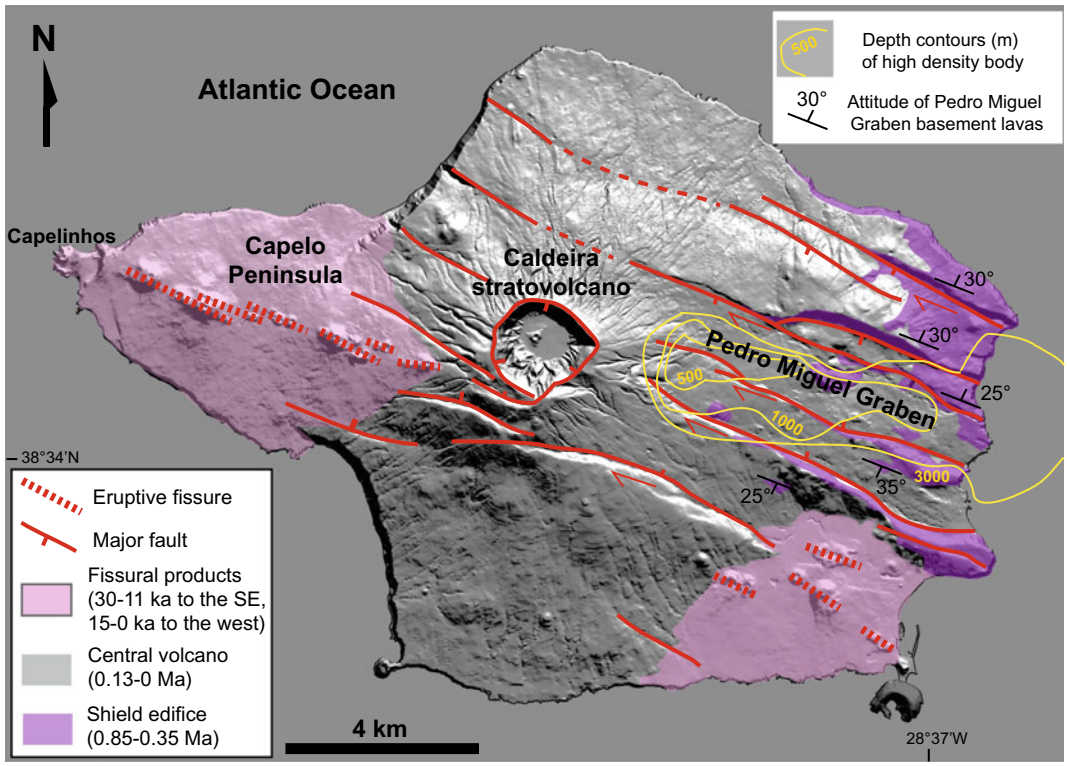

Fig. 13.18 Azores hot spot. Structural map of Faial Island, central Azores, including the Pedro Miguel Graben and its main fault zones, the Caldeira stratovolcano, the Capelo Peninsula and its main fissure eruptions, and the depth contours of the high density body (higher density of >200 kg/m^3) suggesting the presence of a dike complex below the graben (Camacho et al. 2007)

plume responsible for the eastern Azores Islands, although dominated by a source component not evident in the eastern archipelago. Flores consists of overlapping stratovolcanoes, without extended fissure systems. Shallow submarine volcanism occurred between 2.2 and 1.5 Ma. The most voluminous volcanism occurred between 0.7 and 0.5 Ma. Subaerial Corvo has been active between 1–1.5 Ma and 80 ka: its dominant feature is a ~2 km wide and 300 m deep caldera (Genske et al. 2012, and references therein).

13.8 Yellowstone Hot Spot

Yellowstone super-volcano is the most striking and best-known expression of continental hot spot. Large volumes of magma, resulting from the activity of the plume below, were emplaced in western North America to the east of the Juan de Fuca-Farallon subduction system during the last ~20 Ma. Three main magmatic provinces are related to the activity of this plume: the Columbia River Basalts Province, whose magma chambers mark the location of the former plume head, the High Lava Plains of Oregon (or Newberry Hotspot Track), whose western end marks the current plume head, and the Yellowstone Hotspot Track, whose eastern end marks the current plume tail. Such a configuration results from a complex history of plume-slab interaction (Fig. 13.19; Camp and Ross 2004; Wolff et al. 2008).

At ~20 Ma, when the rising Yellowstone plume intersected the overlying eastward-dipping Juan de Fuca-Farallon slab, the plume head flowed westwards, along the upper base of the slab. At ~17 Ma, the plume head punched through the slab and reached the surface, causing volcanism through long and narrow arcuate rifts. Subsequently, the plume head spread out northwards at the base of the lithosphere, probably forced by the thicker cratonic lithosphere boundary to the east, generating the Columbia River Basalts. These consist of ~210,000 km^3 of 17–14 Ma old lava flows and N-S oriented dike swarms. The largest and oldest silicic centres lie along a narrow north-northeast trend at the transition between the craton and accreted oceanic crust. As the North American plate moved southwest, the plume head may have sheared off from the tail and stayed with the plate, trapped by the deeper keel of the older, thicker lithosphere to the east. Contemporaneously, the focused plume tail may have tilted southeast and, by ~15 Ma, propagated northeastward with respect to the North American plate, along the present Eastern Snake River Plain (Xue and Allen 2007; Pierce and Morgan 2009; Obrebski et al. 2010; Coble and Mahood 2012; Camp et al. 2017; Morriss et al. 2020).

The resulting Newberry and Yellowstone tracks show age-progressive volcanism migrating from McDermitt Caldera, which was above the plume head at ~17 Ma. The Newberry Hotspot Track consists of bimodal products with silicic northwest age progression ending in the Newberry volcano (younger than 0.01 Ma), which marks the present location of the plume head, with a propagation rate of 13 km/Ma since 5 Ma. The Yellowstone Hotspot Track is associated with the east-northeast migration of bimodal volcanism along the Eastern Snake River Plain, ending after 800 km at the Yellowstone Caldera, the current tail of the plume (Fig. 13.19; Smith et al. 2009).

Massive rhyolitic volcanism along the Eastern Snake River Plain resulted from basaltic magma differentiation and crustal melting induced by the plume in the last ~16 Ma. The eruptive rate has been fairly uniform since the inception of the Eastern Snake River Plain–Yellowstone volcanic track, between 16 and 17 Ma, with the exception of a gap between 4.5 and 2.1 Ma. In particular, volcanism consisted of frequent (for example peaking every 200–300 ka from 12.7 to 10.5 Ma), high temperature (>1000 °C) and large volume rhyolitic eruptions, with individual ignimbrites reaching 1000 km^3, associated with large calderas. Rhyolites are explained through remelting of their erupted and subvolcanic predecessors on rapid time scales. This volcanism was followed by a similar migration of basaltic lava flows and emplacement of midcrustal mafic intrusions. Finally, the load from the dense intrusions, as well as lithospheric cooling and

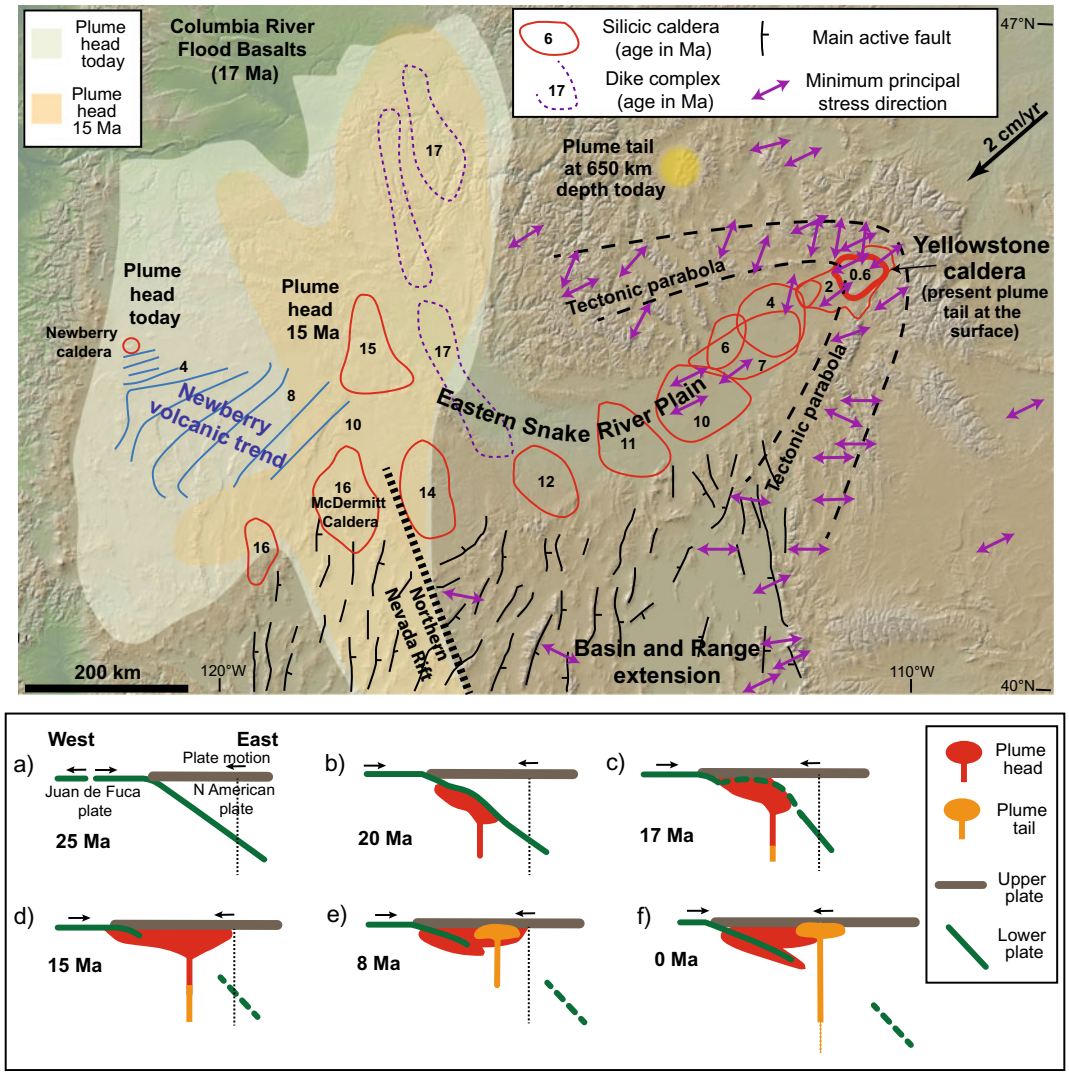

Fig. 13.19 Yellowstone hot spot. Above: overview of the main tectonic and magmatic features of the area affected by the Yellowstone plume, including the distribution of the main volcanic provinces, the current head and tail of the plume and the "tectonic parabola", a region of high seismicity and topography surrounding the Eastern Snake River Plain and the Yellowstone caldera (thick red line). The Newberry volcanic trend highlights local migration of volcanism (blue lines, in Ma). Plate velocity is with regard to the hot spot (modified after Smith et al. 2009). Digital Elevation Model provided by GeoMapApp. Below: proposed model for the interaction between the subducting Juan de Fuca plate and the Yellowstone plume head. **a** 25 Ma, the Yellowstone plume approaches the subducting Juan de Fuca plate; **b** 20 Ma, the plume head has intersected the Juan de Fuca plate and preferentially flowed westwards along the base of the slab; **c** 17 Ma, the plume head has punched through the Juan de Fuca plate, destroyed a larger portion of the slab and caused the volcanism at the surface; **d** 15 Ma, the plume head material spreads out in a larger region at the base of the lithosphere; **e** 8 Ma, the subducting slab drags the remnant plume head material down into the mantle; **f** at present, the hot material from the remnant plume head has been brought to greater depth by the ongoing subducting slab. The vertical dashed line indicates the progression of the current Yellowstone caldera to the west; the orange plume stem represents a hypothetical Yellowstone plume since the arrival of the plume head (shown in red; Xue and Allen 2007)

thermal contraction, has induced, largely before 6.6 Ma, a crustal flexure with 4.5–8.5 km of subsidence along the northeast edge of the plain. Therefore, passage of the North American plate over the melting anomaly has been accompanied by a migrating sequence of events consisting of uplift, regional deformation, massive explosive silicic eruptions and caldera collapse, basaltic volcanism and subsidence (Smith and Braile 1994; McQuarrie and Rodgers 1998; Pierce and Morgan 2009; Knott et al. 2020).

Presently, the Eastern Snake River Plain behaves as a rigid, non-extending block, where much of the minor extension has been accommodated transiently by dikes perpendicular to the plain axis, extending in a NE-SW direction. The Eastern Snake River Plain displays Holocene strain rates one order of magnitude lower than those in the adjacent Basin and Range. The transition zone in between, roughly identified by a parabolic-shaped region ("tectonic parabola"; Fig. 13.19), undergoes dextral and sinistral faulting, associated with seismicity, along the northwest and southeast boundaries of the plain, respectively (Smith and Braile 1994; Parsons et al. 1998; Payne et al. 2012). The ~42 km deep Moho beneath the Eastern Snake River Plain shallows to ~37 km to either side and thickens to ~47 km to the northeast. The lower crust of the plain, generally thickened by a dense underplated layer, shows a low velocity, probably molten layer. This underlies a 4–11 km thick mid crustal high density sill complex of gabbroic lenses interfingering with the granitic upper crust. The amount of mantle-derived mass added to the crust between 11 and 4 Ma is ~340,000 km^3, corresponding to an average mass flux of 0.05 km^3/year, comparable to other hot spots (Peng and Humphreys 1998; McCurry and Rodgers 2009).

Yellowstone caldera constitutes the easternmost active volcanic system fed by the plume tail past the Eastern Snake River Plain. Below Yellowstone caldera, at 60–120 km depth, the plume is sheared southwest by the motion of the North American plate, producing a low velocity layer beneath the thin lithosphere with excess temperature of ~50 to ~200 °C. Below, the plume appears as a ~80 km wide vertical conduit down to 200–300 km depth, where it dips 60° west-northwest, extending to 660 km depth. Upper mantle convection induces eastward flow at ~5 cm/year, that deflects the ascending plume into its west-tilted geometry. The upward deflection of the 660 km deep upper mantle transition zone by 12–18 km over an area ~200 km wide suggests a high-temperature, plume-like upwelling. The upwelling velocity of the plume, characterized by ~2% partial melt, is ~6 cm/year, with a buoyancy flux (0.25 Mg/s) many times smaller than that of oceanic plumes (Xue and Allen 2007; Smith et al. 2009; Schmandt et al. 2012; Tian and Zhao 2012).

The regional signature of the hot spot is currently highlighted by a 600 m high and ~600 km wide topographic bulge centred on Yellowstone caldera, reflecting long-wavelength tumescence (Smith and Braile 1994; Smith et al. 2009). The larger than 15,000 km^3 upper crustal magma reservoir beneath Yellowstone is 6 to 16 km deep, continuing laterally 20 km north of the caldera boundary. Having 2–15% melt, it is assumed as a fluid-saturated porous material consisting of granite and a mixture of rhyolite melt saturated with water and CO_2. In the lower crust, at a depth between 25 and 50 km, a basaltic magma reservoir with a size ~4.5 times that of the upper crustal magma reservoir contains a melt fraction of ~2% and provides the magmatic link between the plume and the upper crustal reservoir (Smith et al. 2009; Huang et al. 2015).

The Yellowstone volcanic field formed during three major caldera-forming rhyolitic eruptions at approximately 2.0, 1.3 and 0.6 Ma, emitting approximately 2500 km^3, 280 km^3 and 1000 km^3 of magma, respectively. The youngest eruption formed the current Yellowstone caldera, followed by ~50 rhyolitic and basaltic events, the youngest at ~70 ka (Fig. 13.20). The composition of the erupted magmas is bimodal, with rhyolitic rocks dominating and basaltic rocks representing a small mostly extra-caldera fraction, and intermediate compositions absent. Silicic magmatism proceeded via shallow-level remelting of earlier erupted and hydrothermally altered source rocks,

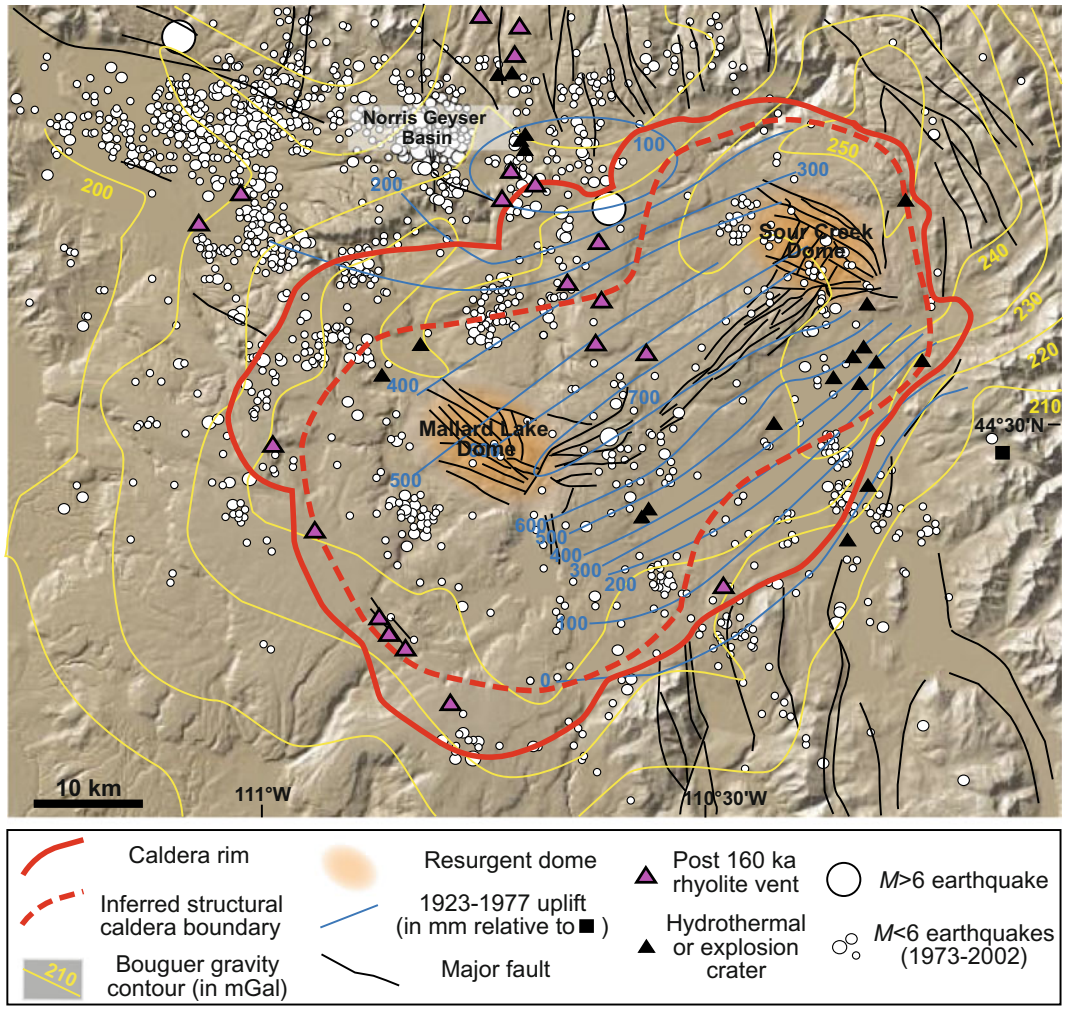

Fig. 13.20 Structure of Yellowstone super-volcano (Wyoming, USA), showing the caldera and its gravity contours, the two resurgent domes, the post-160 ka vents, the uplifted area between 1923–1977 and the 1973–2002 seismicity (after Smith and Braile 1994; Christiansen 2001)

with basaltic magma providing the heat for melting. Analysis of the products of the caldera-forming eruptions reveals a short duration of reservoir assembly, which documents rapid crustal remelting and eruption rates two to three orders of magnitude higher than those of continental arc volcanoes (Smith and Braile 1994; Christiansen 2001; Bindeman et al. 2008; Wotzlaw et al. 2015). The 40 × 70 km wide and ~2 km deep caldera hosts two intensely fractured resurgent domes (Sour Creek and Mallard Lake). The caldera coincides with a −60 mGal gravity anomaly. Focal depths of earthquakes decrease from more than 11 km outside this anomaly to less than 6 km within, reflecting thinning and heating of the seismogenic crust (Miller and Smith 1999). The most striking surface expression of the current activity of the caldera is its huge hydrothermal system, which contains more than 10,000 thermal features, including the world's greatest concentration of geysers, hot springs, mudpots, and steamvents (Fig. 13.21).

Fig. 13.21 Yellowstone hot spot. View of the Grand Prismatic Spring in Midway Geyser Basin at Yellowstone on October 19, 2017. *Photo credit* U.S. Geological Survey, USGS

13.9 Tibesti Hot Spot

The Tibesti hot spot lies in northern Chad, northern Africa. Northern Africa contains several hot spots characterized by anomalous topographic swells and intraplate Cenozoic volcanism, as Hoggar (Algeria), Darfur (Sudan), Cameroon (Cameroon) and Tibesti (Fig. 10.18). Rather than reflecting the involvement of one or several deep mantle plumes, or even a connection with the nearby larger Afar hot spot, these intraplate hot spots are probably related to unconnected plumes and attributed to shallow processes. In particular, the Tibesti hot spot does not show any seismic signature in the upper mantle, suggesting a shallower asthenospheric origin (Pik et al. 2006; Sebai et al. 2006). The low shear velocities at 100–150 km depth in this region can be interpreted in terms of elevated temperatures due to a shallow plume, whose stem appears to migrate approximately 100 km to the west between depths of 100 and 150 km. At shallow levels this plume may also feed the volcanism of the nearby Al Haruj region to the north, in Libya (Keppie et al. 2010). Thermobarometric and tomographic studies suggest that asthenospheric temperatures beneath Al Haruj in the last 5 Ma are more than 50 °C hotter than ambient mantle and 20–40 °C hotter than those predicted to be present beneath the Tibesti region. In addition to the elevated asthenospheric temperature, a contribution from lithospheric melting related to the Cretaceous rifting of the Sirt Basin (Libya), associated with lithospheric thinning, has been inferred for both regions (Cvetkovi et al. 2010; Ball et al. 2019).

The Tibesti swell consists of a ~1000 km wide area with altitudes generally of ~1000 m above the surrounding areas, with several volcanoes with elevation above 2000 m. This positive relief coincides with a geological uplift exposing Precambrian rocks surrounded by Phanerozoic rocks. River profiles suggest that most uplift (0.4–1.2 km) occurred at ~30 Ma, whereas the more recent uplift is estimated at less than 0.4 km. The produced dome is inferred to result from the anomalously hot asthenosphere, which upwells beneath the lithosphere (Keppie et al. 2010; Roberts and White 2010).

The Tibesti hot spot likely lies along a ~6000 km long NW–SE striking lineament (Tibesti Lineament), extending from southwest Algeria to Kenya. This corresponds to a 200–300 km wide fault zone with a possible late Proterozoic origin and reactivated as a transtensive dextral system during hot spot volcanism (Guiraud et al. 2000; Nkono et al. 2018). Despite this probable regional tectonic contribution, the Tibesti region has been aseismic, at least above *M5.5*.

The hot spot-induced Tibesti Volcanic Province (TVP) consists of several shield volcanoes (up to 80 km diameter) with large-scale calderas, extensive lava plateaux and flow fields, and widespread ignimbrite deposits (Fig. 13.22; Permenter and Oppenheimer 2007; Deniel et al. 2015). The composition of magma is mainly bimodal, with basalts representing roughly 60% in volume and felsic rocks, such as rhyolites,

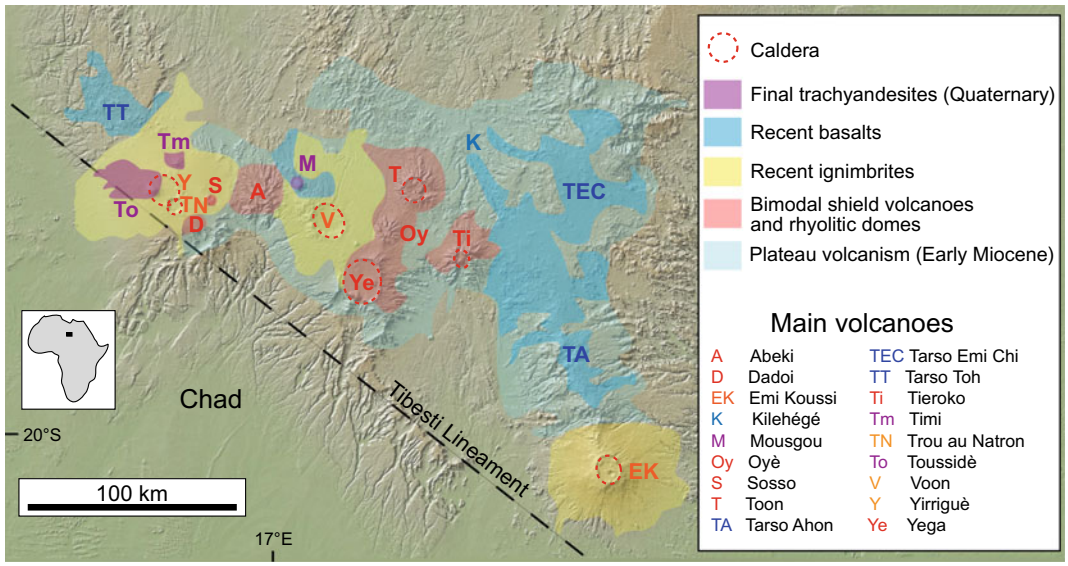

Fig. 13.22 Simplified map of the Tibesti Volcanic Province, Chad (location in inset), with products ranging from the plateau volcanism (approximately 17 Ma) to the final Quaternary volcanism. Labels of major volcanoes have the same colour as the related stage of activity of the province shown above (modified after Gourgaud and Vincent 2004; Deniel et al. 2015)

trachytes, and minor phonolites, approximately 40%. Intermediate compositions, mostly trachyandesites, represent less than 1% volume, and are only encountered in the final volcanic activity. The activity of the TVP began as early as the Oligocene, though the major products that mark its surface date from Lower Miocene to Quaternary. Between at least 17 and 8 Ma widespread alkaline plateau volcanism consisted of flood basalts and silicic lava plugs with intercalated alkaline, peralkaline and rhyolitic ignimbritic sheets. In this period ages of volcanism decrease from northeast to southwest, following the migration of NW–SE trending flexures associated with the Tibesti Lineament and concentrating the feeding dike swarms. Late Miocene large central composite tholeiitic volcanoes, some of which (Toon, Oyé, and Yéga) NNE-SSW aligned, formed in the central part of the TVP. After this initial phase of activity in the central TVP, volcanism migrated to both the eastern and western TVP regions, showing a relatively haphazard spatial development. This is mainly testified by the construction of three large alkaline, peralkaline and rhyolitic ignimbritic volcanoes, associated with significant updoming of the basement, ending with the collapse of large calderas: Voon (5–7 Ma), Emi Koussi (2.4–1.33 Ma) and Yirrigué (0.43 Ma). Basaltic activity, starting at about 5–7 Ma, and essentially consisting of cinder cones and associated lava flows, also occurred to the west and southeast of the TVP (Tarso Tôh, Tarso Ahon, and Tarso Emi Chi). The final volcanic activity is represented by post-Yirrigué caldera activity in the Tarso Toussidé Volcanic Complex and especially Toussidé (the only active volcano in Tibesti), Timi and Mousgou volcanoes (Permenter and Oppenheimer 2007; Deniel et al. 2015, and references therein).

Volcanism of the TVP has been poorly studied in detail, with the above-mentioned Emi Koussi representing one of the best-known volcanoes of the hot spot. This consists of a wide ignimbritic shield-like volcano resulting from the succession of three eruptive sequences, each related to caldera collapse. Its products exhibit two bimodal lava series, silica-saturated and silica-undersaturated, with a wide compositional gap (of $\sim$10% SiO_2). While the silica-saturated

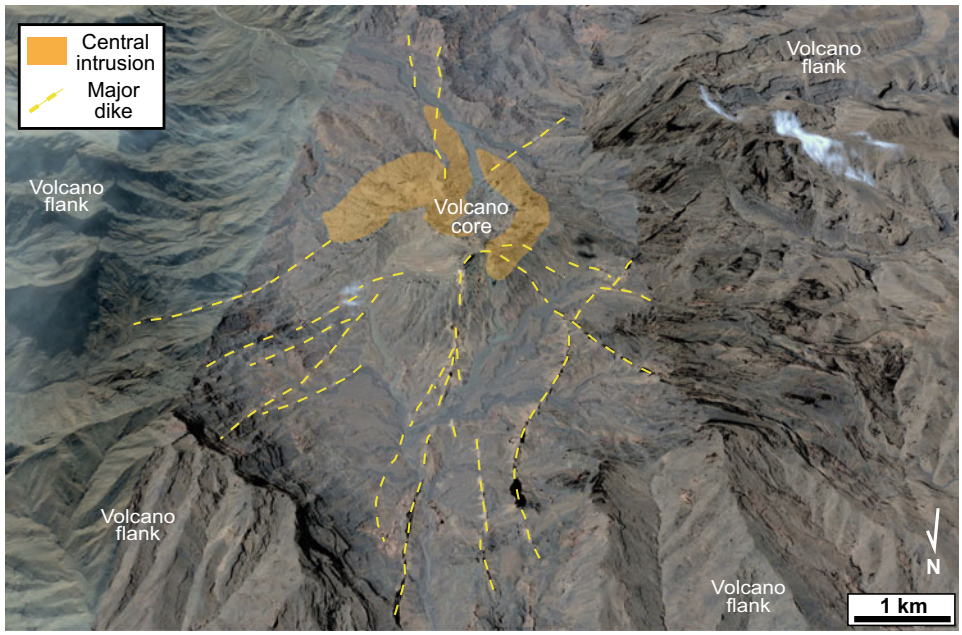

Fig. 13.23 Tibesti hot spot. Google Earth image of the eroded Tieroko volcano, as seen from the north. The eroded central portion of the composite volcano reveals its dike pattern radiating from one or more central intrusions (image source: Google Earth)

suite may be explained by crustal contamination, the undersaturated suite may be explained by crystal fractionation (Gourgaud and Vincent 2004).

The volcanoes of the Tibesti hot spot do not show clear evidence of defined rift zones or significant flank failure, at least from remote sensing data. However, unusual conditions of uplift and erosion currently enable exceptional exposure of the internal structure of some volcanoes. Indeed, the eroded portions of several volcanoes reveal NW–SE trending feeder dikes, associated with flexures, and radial dike patterns. The latter are best developed at Kilehégé, where more than a hundred rhyolitic dikes, 3–15 m thick, converge toward a focal zone with the highest spines and several rhyolitic plugs, and at Tiéroko, where the radial dikes are similarly associated with a central intrusion (Fig. 13.23; Deniel et al. 2015).

As mentioned, a distinctive feature of the Tibesti hot spot is the lack of any clear spatial progression of volcanic centres, though volcanism seems to have initiated in the Central region (e.g. Voon and Toon) and later migrated to the eastern and western regions: this feature is also matched by the lack of a linear hot spot track. In addition, this sparse magmatic activity produced a wide variety of volcanic features, including moderate to large-scale calderas (average diameter of $\sim$12 km), suggesting also significant magma reservoirs below (Permenter and Oppenheimer 2007).

13.10 Comparing Hot Spot Volcanoes

Hot spots display overall common structural and magmatic features, but also variability in terms of plume structure and magma supply, interaction with the lithosphere, distribution, age and type of volcanism, evolution and structure of the volcanoes. These similarities and differences are

discussed below, also including knowledge from additional examples of hot spots (Table 13.1). Note that the available information on oceanic hot spot volcanoes mainly concerns their subaerial tips: therefore, the limited knowledge of their submerged portions may affect the considerations made in the following discussion.

A common feature of oceanic and continental hot spots is the geophysical detection of underplated magma, more voluminous than the erupted portion. A broad surface swell is usually, but not systematically, accompanied with magmatic underplating, as at Hawaii, Reunion, the Canary Islands, Yellowstone, Tibesti and in the South Pacific, at both a regional (superswell) and local scale (volcanic chain or cluster; Sichoix et al. 1998; Suetsugu et al. 2009; King and Adam 2014; Park and Rye 2019). The swell may be the surface expression of the flexure induced by the emplacement of the underplated magma and/or the upward pressure exerted by the plume head.

Another common feature of the considered hot spots, with the possible exception of the Canary Islands, is the influence of pre-existing basement structures on volcanic activity. This occurs both on continental and oceanic lithosphere, where any pre-existing discontinuities (faults, fracture zones) may be reactivated and/or intruded by magma. This control of inherited structures, recognized also in the Iceland, Afar and French Massif Central hot spots, indicates that hot spot volcanism is affected by regional structures and/or stresses. The reactivation of regional anisotropies often results in the control of the location, alignment and shape of hot spot volcanoes, including their rift zones and flank instabilities.

Radial volcanic rift zones are common at oceanic hot spots, although their configuration and overall architecture vary widely. On the Hawaiian Islands, the well-developed rift zones consist of long and narrow portions of focused magmatic injection controlled by pre-existing structures, edifice morphology, and flank instability. The best-known Hawaiian rift zones (on Mauna Loa and Kilauea) developed at the head of the unstable flanks of the volcanoes, although the longest rifts extend far beyond the shield edifice, probably also following basement fractures. In contrast, rift zones are poorly developed on the western Galapagos volcanoes or on Easter Island, where diffuse areas of radial dike injection predominate. In between are the defined but relatively wide rift zones of Reunion, which further widen downslope, and the rift zones forming triple arms at 120° mainly on the younger Canary Islands volcanoes, often at the head of collapse structures. In other cases (Azores, the eastern Galapagos Islands), the rift zones are aligned along pre-existing regional trends or anyway highlight the influence of plate boundary stresses. Therefore, the presence and development of rift zones on oceanic hot spots may be reconciled, in addition to the local stress field imposed by the volcanic edifice, with unstable flanks, pre-existing structures and regional stresses. Available evidence (Koolau, Kilauea and Mauna Loa in the Hawaiian Islands, Fernandina in the Galapagos Islands, Tenerife and El Hierro in the Canary Islands, Sao Jorge in the Azores) suggests a predominant lateral propagation of the dikes feeding the rift zones. No evident rift zones have been found in the considered continental hot spots.

Oceanic hot spot volcanoes also show widespread (though not ubiquitous) instability, often resulting in catastrophic collapse. This has been documented in the Hawaiian Archipelago, the Canary Islands, the Azores, Reunion Island and the South Pacific Islands (Tahiti and the Marquesas volcanic chain). In some cases (Canary Islands, Reunion, Marquesas) flank instability results in widespread mass wasting. On the Galapagos Archipelago (with the exception of Ecuador volcano) and Easter Island flank instability is negligible. The general lack of flank instability at the Galapagos volcanoes may be related to their shallow submarine flanks perched on the Galapagos Platform, and/or to the young age of the oceanic lithosphere below the platform, which has hindered the accumulation of clayish oceanic deposits: elsewhere, as below Hawaii, these weak water-saturated deposits may act as decollement level for the volcanic edifices.

Table 13.1 Summary of the regional and local tectonic and magmatic features related to hot spot volcanoes; with the exception of Yellowstone and Tibesti, all listed hot spots are located on oceanic crust

Hot spot	Age of crust (Ma)	Plate velocity (cm/year)	Eruptive rate (km^3/Ma)	Buoyancy flux (Mg/s)	Composition (SiO_2 wt%)	Volcano distribution	Elevation above ocean floor (m)	Rift zones	Summit caldera	Flank instability
Hawaii	80	8.6	10^5	7.10	39–61	Aligned	5000 + 4300	Focused	Yes	Yes
Society	60	10	10^2–10^3	2.72	42–49	Aligned	4000 + 2200	Focused	(Yes)	Yes
Galapagos	8	5.9	10^3	0.71	45–51	Scattered	3500 + 1700	Diffuse	Yes	(No)
Easter	2–4	13.3	0.01–100	0.43	41–74	Aligned	3500 + 500	Diffuse	Yes	No
Réunion	60	1.9	3.4×10^3	0.08	45–70	Aligned	4300 + 3050	(Focused)	Yes	Yes
Canary	160–180	1.9	10^3–10^4	0.13	36–73	Scattered	3600 + 3700	Focused	Yes	Yes
Azores	9–10	2	10^3	0.48	44–65	Scattered	3400 + 2350	Focused	Yes	(Yes)
Madeira	130–140	1.2	10^2–10^3	0.22	41–54	Aligned	4500 + 1850	Focused	No	Yes
Ascension	7	1.7	30	0.09	46–75	Aligned	3500 + 860	Diffuse	No	Minor
Yellowstone	>2500	2	2.5×10^3	0.25	43–79	Aligned	0 + 3400	N/A	Yes	No
Tibesti	>550	1.9	3×10^2	0.51	43–66	Scattered	0 + 3450	N/A	Yes	No

Elevation above seafloor results from depth of ocean (left column) and height above sea level (right column) of the highest volcano in the hot spot. Brackets indicate that the specified feature may not be completely represented (modified from Vezzoli and Acocella 2009; King and Adam 2014)

At Easter Island the lack of flank instability may be attributed to the lower output rate of the hot spot, which builds less imposing volcanic edifices.

There is an overall association between focused volcanic rift zones and unstable volcano flanks (at Hawaii, Society Islands and Canary Islands), as well as between diffuse rift zones and stable flanks (Galapagos, Easter Island). This suggests an interaction where flank instability focuses magmatic activity in rift zones at the head of the unstable flank, preferably of a large volcano, with magmatic activity along rift zones in turn enhancing further instability. At the Azores, the development of the rift zones seems more controlled by the regional structures, rather than flank instability.

The summits of oceanic and continental hot spot volcanoes are also characterized by calderas, as observed on all the above-mentioned examples, as well as in the South Pacific volcanic chains. A few of these summit calderas (Galapagos and, to a much lesser extent, Reunion and Easter Island) are associated with dike-fed circumferential eruptive fissures, rarely documented elsewhere. In addition, the summits of a few oceanic hot spot volcanoes (Tenerife, Reunion and Fogo, Cape Verde) show distinctive horseshoe-shaped scarps continuing on the volcano flanks, probably associated with a complex interplay between vertical and lateral collapse.

Despite these general similarities, hot spot volcanoes also show striking differences in both evolution and structure, with a variability pointing to a growth and architecture that are more complex than those proposed for example for the reference Hawaiian hot spot.

Among the differences in the considered hot spots, a first-order feature is the distribution of localized or delocalized volcanism. In fact, in some cases (Galapagos, Canary Islands, Azores, Tibesti) volcanic activity and volcano growth are synchronous, or scattered, developing several coalesced coeval volcanoes. In others (Hawaii, Reunion, Yellowstone), the activity and growth of the volcanoes are sequential, or aligned, with only a few neighbouring volcanoes active at the same time. Intermediate hybrid types of activity and growth characterize some volcanic chains of the South Pacific. Such an aligned or scattered distribution of volcanism is illustrated by the focused vs. diffuse age-distance relationships shown in Fig. 13.24. These different distributions of the hot spot volcanoes may have various explanations. The distributions may reflect different types of plumes: for example, a superplume fed by different plumelets, as below the Cook-Austral Islands, may generate a scattered distribution of volcanoes more easily than a single plume, as below Reunion (e.g., Koppers et al. 2003). Absolute plate velocity may be an additional feature controlling the duration and persistence of a feeding system below a volcano, with faster plates favouring aligned volcanism (Hawaii, Society Islands in the South Pacific) and slower plates encouraging scattered volcanism (Canary Islands, Azores, Tibesti; Mitchell et al. 2002). A third control may be the age, and the related thickness, of the oceanic lithosphere above the hot spot (Poland 2014). For example, the thicker lithosphere may induce focused volcanism in Hawaii and the thinner lithosphere dispersed volcanism in Galapagos, with both hot spots lying on plates with medium–high velocity. In fact, despite the lower buoyancy flux of the Galapagos plume, a thinner (younger) lithosphere may be more effectively heated and weakened by a mantle plume, developing multiple magmatic paths and thus showing delocalized volcanism. Within an adequate tectonic context, as in proximity to a triple junction, scattered magmatism may develop a microplate with non-rigid behaviour, as observed in the Azores. A fourth factor possibly influencing the aligned or scattered distribution of volcanoes is the magma flux of the hot spot. This is suggested by the more aligned distribution of volcanoes on the less productive Madeira hot spot with regard to that of the nearby and more productive Canary Islands hot spot, both in a similar tectonic setting (Table 13.1 and Fig. 13.24; Geldmacher et al. 2000).

Also, while a swell has been recognized below most hot spot volcanoes, a moat due to the

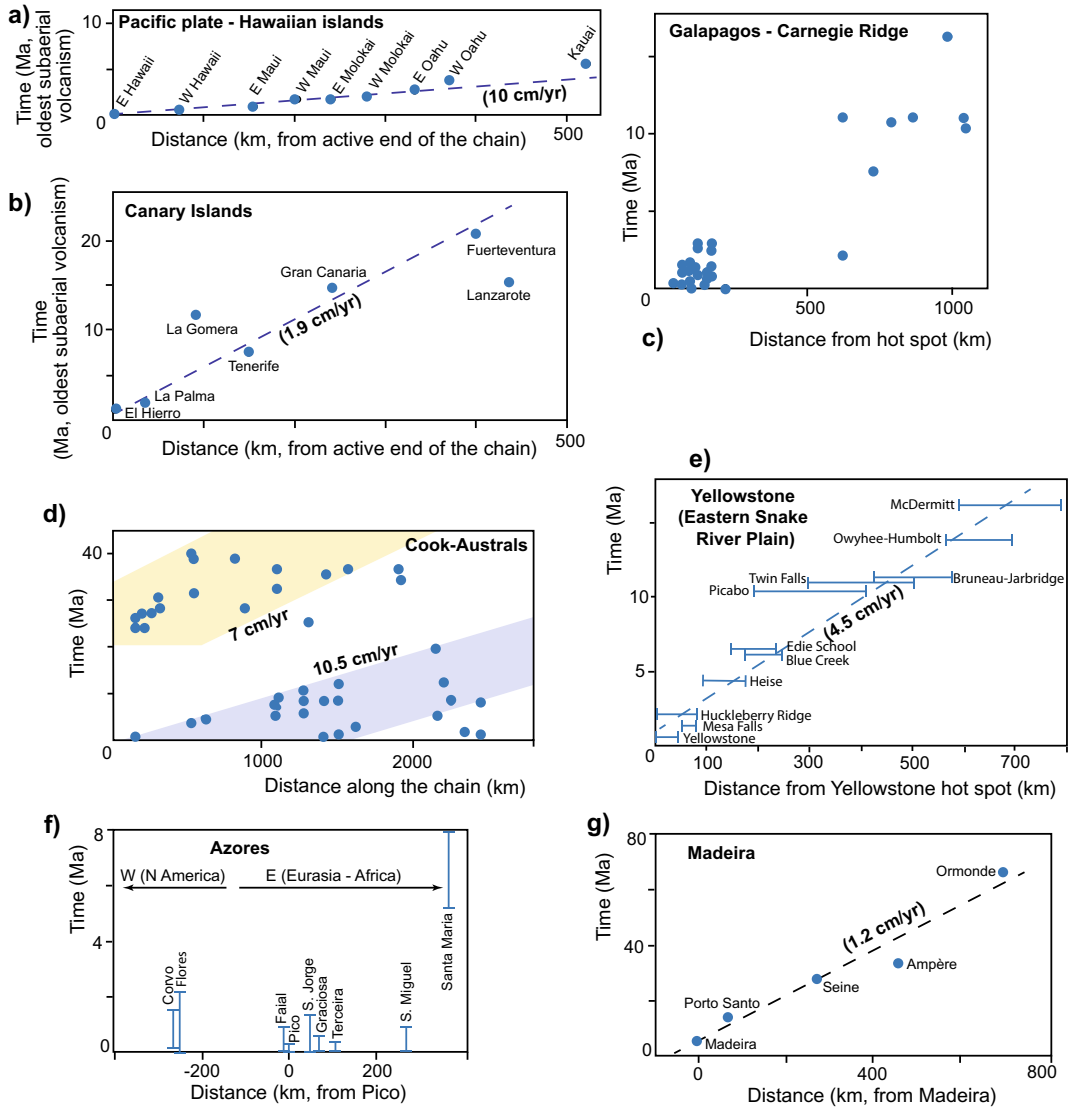

Fig. 13.24 Age of volcanism with regard to the distance from the hot spot location for several hot spots: **a** Hawaiian Islands; **b** Canary Islands; **c** Galapagos-Carnegie Ridge; **d** Cook-Australs; **e** Yellowstone; **f** Azores; **g** Madeira. While several host spots (as Hawaii, Madeira, Yellowstone) show a defined age-distance relationship, implying aligned volcanism, others (as Cook-Australs, Galapagos, Azores) show a more dispersed distribution, implying scattered volcanism

load of the volcanic edifices appears less frequent. A moat has been detected around the volcanoes of Hawaii, Tenerife, and, in part, below the Galapagos, the South Pacific and the Canary Islands: conversely, no moat has been recognized around the Azores and Reunion volcanoes.

A further notable difference in the eruptive style and composition of hot spot volcanoes is related to the nature of their lithosphere. Bimodal compositions, as well as explosive activity related to the evolved magmas, are more common on continental hot spots. At Yellowstone the plume triggers bimodal volcanism, first melting the

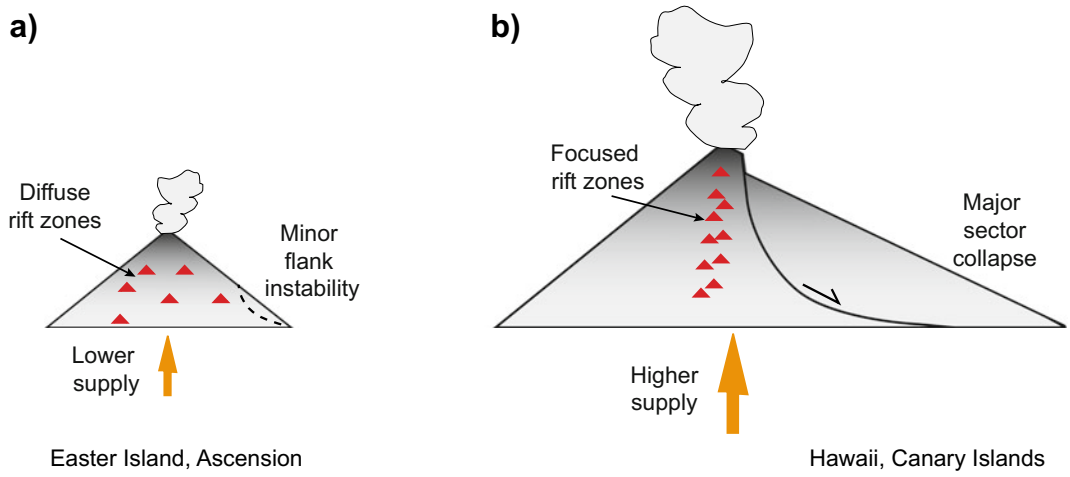

Fig. 13.25 Working hypothesis showing how the structural features (in terms of sector collapses and rift zones to the rear of the collapses) of end-member oceanic hot spots volcanoes depend upon their magma supply and size. **a** Lower magma supplies generate smaller volcanoes with minor flank instability and diffuse rift zones. **b** Higher magma supplies generate larger volcanoes with major sector collapse and focused rift zones. Here only the subaerial portion of the edifice is reported, not to scale

silicic continental crust, producing rhyolites with explosive activity, and then erupting the more primitive products. Tibesti also shows bimodal volcanism, although the rhyolitic compositions are proportionally much less represented than Yellowstone, probably following a more limited crustal melting. Rhyolites and explosive eruptions are usually rare on oceanic hot spots, except in the Canary Islands, Alcedo (Galapagos) and Terceira (Azores). Oceanic hot spot volcanoes are indeed characterized by the predominant effusive activity of mafic magma.

Despite all the differences in the oceanic hot spot volcanoes discussed above, probably the most striking one concerns their extremely variable eruptive rates. Considering the general limitation that estimates for oceanic volcanoes mainly refer to their subaerial tip, the eruptive rates vary over several orders of magnitude, from Hawaii ($\sim 10^5$ km^3/Ma) to Ascension or Easter Island (the latter reaching 10^{-2} km^3/Ma) (Table 13.1). While the highest eruptive rates at Hawaii are associated with focused rift zones and significant lateral collapse, at Easter Island and Ascension the low eruptive rates are mainly accompanied with poorly defined, diffuse rift zones and minor flank instability. These end-member behaviours suggest a complex and not yet fully understood interplay between magma flux, maturity of rift zones and flank instability. A working hypothesis relates these end-member oceanic behaviours to the magma supply and the size of the volcanic edifice. Accordingly, the more productive and larger volcanic edifices generate significant flank instability and focused rift zones, whereas less productive and smaller edifices have minor or no flank instability and diffuse rift zones (Fig. 13.25; Vezzoli and Acocella 2009). The western Galapagos Islands provide an exception, as characterized by high productivity, but lacking flank instability and focused rift zones. This feature may be explained by the relatively small size of the volcanoes and/or their stronger basement, with a thick platform overlying a young oceanic lithosphere lacking the clayish sediments that may promote a basal decollement.

13.11 Summary

Hot spots are the surface expression of plumes upwelling from the Earth's mantle, most often appearing on oceanic lithosphere. Volcanic

activity related to representative hot spots shows major recurrent features and differences.

Recurrent features of oceanic and continental hot spot volcanoes include widespread underplating, influence of pre-existing basement structures and the development of volcanic edifices with summit caldera. Oceanic hot spots also show frequent radial rift zones, often accompanied by flank instability. Major differences among hot spot volcanoes, both in oceanic and continental examples, are related to their distribution (aligned or scattered), eruption rate (varying over several orders of magnitude) and composition (with continental examples showing also widespread rhyolites).

The variability of hot spot volcanoes results from differences in the plume structure and supply, and in the age, rate of motion and nature of lithosphere pierced by the plume: the interplay between these features determines different distributions and types of volcanism, as well as different structure and evolution of the volcanoes. In general, the larger the magmatic output of oceanic hot spots, the larger are the islands and the more developed are the instability of the volcanoes flanks and the rift zones, with Hawaii and Easter Island representing end-member behaviours and the Galapagos Islands providing an exception.

References

Abratis M, Schmincke HU, Hansteen TH (2002) Composition and evolution of submarine volcanic rocks from the central and western Canary Islands. Int J Earth Sci 91:562–582

Acosta J, Uchupi E, Smith D, Munoz A, Herranz P, Palomo C et al (2003) Comparison of volcanic rifts on La Palma and El Hierro, Canary Islands and the Island of Hawaii. Mar Geophys Res 24:59–90

Albarede F, Luais B, Fitton G, Semet M, Kaminski E, Upton BGJ et al (1997) The geochemical regimes of Piton de la Fournaise volcano (Reunion) during the last 530,000 years. J Petrol 38:171–201

Ancochea E, Brandle JL, Cubas CR, Hernan F, Huertas MJ (1996) Volcanic complexes in the eastern ridge of the Canary Islands: the Miocene activity of the island of Fuerteventura. J Volcanol Geoth Res 70:183–204

Bagnardi M, Amelung F (2012) Space-geodetic evidence for multiple magma reservoirs and subvolcanic lateral intrusions at Fernandina Volcano, Galápagos Islands. J Geophys Res 117:B10406. https://doi.org/10.1029/2012JB009465

Bagnardi M, Amelung F, Poland MP (2013) A new model for the growth of basaltic shields based on deformation of Fernandina volcano, Galápagos Islands. Earth Planet Sci Lett 377–378:358–366

Ball PW, White NJ, Masoud A, Nixon S, Hoggard MJ, Maclennan J et al (2019) Quantifying asthenospheric and lithospheric controls on mafic magmatism across North Africa. Geochem Geophys Geosyst 20. https://doi.org/10.1029/2019GC008303

Barruol G, Fontaine FR (2013) Mantle flow beneath La Reunion hot spot track from SKS splitting. Earth Planet Sci Lett 362:108–121

Becerril L, Galindo I, Marti J, Gudmundsson A (2015) Three-armed rifts or masked radial pattern of eruptive fissures? The intriguing case of El Hierro volcano (Canary Islands). Tectonophysics 647–648:33–47

Bianco TA, Ito G, Beker JM, Garcia MO (2005) Secondary Hawaiian volcanism formed by flexural arch decompression. Geochem Geophys Geosyst 6: Q08009. https://doi.org/10.1029/2005GC000945

Bindeman IN, Fu B, Kita NT, Walley JW (2008) Origin and evolution of silicic magmatism at yellowstone based on ion microprobe analysis of isotopically zoned zircons. J Petrol 49:163–193

Bird P (2003) An updated digital model of plate boundaries. Geochem Geophys Geosyst 4:1027. https://doi.org/10.1029/2001GC000252

Blahut J, Mitrovic-Woodell I, Baron I, Rene M, Rowberry M, Blard P-H et al (2020) Volcanic edifice slip events recorded on the fault plane of the San Andrés Landslide, El Hierro, Canary Islands. Tectonophysics 776:228317

Bonali FL, Corazzato C, Tibaldi A (2011) Identifying rift zones on volcanoes: an example from La Réunion island, Indian Ocean. Bull Volcanol 73:347–366

Bonneville A, Von Herzen RP, Lucazeu F (1997) Heat flow over Reunion hot spot track: additional evidence for thermal rejuvenation of oceanic lithosphere. J Geophys Res 102:22731–22747

Boulesteix T, Hildenbrand A, Soler V, Quidelleur X, Gillot PY (2013) Coeval giant landslides in the Canary Islands: Implications for global, regional and local triggers of giant flank collapses on oceanic volcanoes. J Volcanol Geoth Res 257:90–98

Camacho AG, Nunes JC, Ortiz E, Franca Z, Vieira R (2007) Gravimetric determination of an intrusive complex under the Island of Faial (Azores): some methodological improvements. Geophys J Int 171:478–494

Camp VE, Ross ME (2004) Mantle dynamics and genesis of mafic magmatism in the intermontane Pacific Northwest. J Geophys Res 109:B08204. https://doi.org/10.1029/2003JB002838

Camp VE, Ross ME, Duncan RA, Kimbrough DL (2017) Uplift, rupture, and rollback of the Farallon slab reflected in volcanic perturbations along the Yellowstone adakite hot spot track. J Geophys Res 122:7009–7041

Canales JP, Ito G, Detrick RS, Sinton J (2002) Crustal thickness along the western Galapagos spreading Center and the compensation of the Galapagos hotspot swell. Earth Planet Sci Lett 203:311–327

Carracedo JC (1999) Growth, structure, instability and collapse of Canarian volcanoes and comparisons with Hawaiian volcanoes. J Volcanol Geoth Res 94:1–19

Carracedo JC, Day S, Guillou H, Rodriguez Badiola E, Canas JA, Perez Torrado FJ (1998) Hotspot volcanism close to a passive continental margin: the Canary Islands. Geol Mag 135:591–604

Carracedo JC, Rodriguez Badiola E, Guillou H, Paterne M, Scaillet S, Perez Torrado FJ et al (2007) Eruptive and structural history of Teide Volcano and rift zones of Tenerife, Canary Islands. Geol Soc Am Bull 119:1027–1051

Chadwick WW, Howard KA (1991) The pattern of circumferential and radial eruptive fissures on the volcanoes of Fernandina and Isabela islands, Galapagos. Bull Volcanol 53:259–275

Chadwick WW, De Roy T, Carrasco A (1991) The September 1988 intracaldera avalanche and eruption at Fernandina volcano, Galapagos Islands. Bull Volcanol 53:276–286

Chadwick WW, Geist DJ, Jonsson S, Poland M, Johnson DJ, Meertens CM (2006) A volcano bursting at the seams: inflation, faulting, and eruption at Sierra Negra volcano, Galápagos. Geology 34:1025–1028

Chadwick WW, Jonsson S, Geist DJ, Poland M, Johnson DJ, Batt S et al (2011) The May 2005 eruption of Fernandina volcano, Galápagos: the first circumferential dike intrusion observed by GPS and InSAR. Bull Volcanol 73:679–697

Chaput M, Famin V, Michon L (2014) Deformation of basaltic shield volcanoes under cointrusive stress permutations. J Geophys Res 119:274–301

Charvis P, Laesanpura A, Gallart J, Hirn A, Lepine JC, de Voogd B et al (1999) Spatial distribution of hotspot material added to the lithosphere under La Reunion, from wide-angle seismic data. J Geophys Res 104:2875–2893

Chen K, Smith JD, Avouac J-P, Liu Z, Song YT, Gualandi A (2019) Triggering of the Mw 7.2 Hawaii earthquake of 4 May 2018 by a dike intrusion. Geophys Res Lett 46:2503–2510

Christiansen RL (2001) The quaternary and pliocene yellowstone plateau volcanic field of Wyoming, Idaho, and Montana. US Geological Survey Professional Paper 729-G 145 pp

Clague DA, Sherrod DR (2014) Growth and degradation of Hawaiian volcanoes. In: Poland MP, Takahashi TJ, Landowski CM (eds) Characteristics of Hawaiian volcanoes. US geological survey professional paper, vol 1801, pp 98–146

Clague DA, Paduan JB, Caress DW, Moyer CL, Glazer BT, Yoerger DR (2019) Structure of Loihi Seamount, Hawai'i and Lava flow morphology from high-resolution mapping. Front Earth Sci 7:58. https://doi.org/10.3389/feart.2019.00058

Coble MA, Mahood GA (2012) Initial impingement of the Yellowstone plume located by widespread silicic volcanism contemporaneous with Columbia River flood basalts. Geology 40:655–658

Collier JS, Watts AB (2001) Lithospheric response to volcanic loading by the Canary Islands: constraints from seismic reflection data in their flexural moat. Geophys J Int 147:660–676

Corbi F, Rivalta E, Pinel V, Maccaferri F, Bagnardi M, Acocella V (2015) How caldera collapse shapes the shallow emplacement and transfer of magma in active volcanoes. Earth Planet Sci Lett 431:287–293

Costa ACG, Marques FO, Hildebrand A, Sibrant AIR, Catita CMS (2014) Large-scale catastrophic flank collapses in a steep volcanic ridge: the Pico-Faial Ridge, Azores Triple Junction. J Volcanol Geoth Res 272:111–125

Cullen A, McBirney AR (1987) The volcanic geology and petrology of Isla Pinta, Galapagos archipelago. Geol Soc Am Bull 98:294–301

Cvetkovi V, Toljic M, Ammar MA, Rundic L, Trish KB (2010) Petrogenesis of the eastern part of the Al Haruj basalts (Libya). J Afr Earth Sc 58:37–50

Danobeitia JJ, Canales JP (2000) Magmatic underplating in the Canary Archipelago. J Volcanol Geoth Res 103:27–41

Day SJ, Carracedo JC, Guillou H (1997) Age and geometry of an aborted rift flank collapse: the San Andres fault system, El Hierro, Canary Islands. Geol Mag 134:523–537

Day SJ, Heleno da Silva SIN, Fonseca JFBD (1999) A past giant lateral collapse and present-day flank instability of Fogo, Cape Verde Islands. J Volcanol Geoth Res 94:191–218

Delaney PT, Fiske RS, Miklius A, Okamura AT, Sako MK (1990) Deep Magma body beneath the summit and Rift Zones of Kilauea Volcano, Hawaii. Science 247:1311–1316

DeMets C, Gordon RG, Argus DF (2010) Geologically current plate motions. Geophys J Int 181:1–80

Deniel C, Vincent PM, Beauvillain A, Gourgaud A (2015) The Cenozoic volcanic province of Tibesti (Sahara of Chad): major units, chronology, and structural features. Bull Volcanol 77:74

Dieterich JH (1988) Growth and persistence of Hawaiian volcanic rift zones. J Geophys Res 93:4258–4270

Dumont M, Peltier A, Roblin E, Reninger P-A, Barde-Cabusson S, Fininzola A et al (2019) Imagery of internal structure and destabilization features of active volcano by 3D high resolution airborne electromagnetism. Sci Rep 9:18280. https://doi.org/10.1038/s41598-019-54415-4

Farnetani CG, Hofmann AW (2010) Dynamics and internal structure of the Hawaiian plume. Earth and Planetary Science Letters 295:231–240

Fernandes RMS, Bastos L, Miranda JM, Lourenco N, Ambrosius BAC, Noomen R et al (2006) Defining the plate boundaries in the Azores region. J Volcanol Geoth Res 156:1–9

Fernandez C, Casillas R, Garcia Navarro E, Gutierrez M, Camacho MA, Ahijado A (2006) Miocene rifting of Fuerteventura (Canary Islands). Tectonics 25:TC6005. https://doi.org/10.1029/2005TC001941

Fiske RS, Jackson ED (1972) Orientation and growth of Hawaiian volcanic rifts. Proc R Soc Lond 329:299–326

Fullea J, Camacho AG, Negredo AM, Fernandez J (2015) The Canary Islands hot spot: new insights from 3D coupled geophysical–petrological modelling of the lithosphere and uppermost mantle. Earth Planet Sci Lett 409:71–88

Gailler L-S, Lenat J-F (2012) Internal architecture of La Réunion (Indian Ocean) inferred from geophysical data. J Volcanol Geoth Res 221–222:83–98

Galetto F, Bagnardi M, Acocella V, Hooper A (2019) Noneruptive unrest at the caldera of Alcedo Volcano (Galápagos Islands) revealed by InSAR data and geodetic modelling. J Geophys Res 124. https://doi.org/10.1029/2018JB017103

Gallart J, Driad L, Charvis P, Sapin M, Hirn A, Diaz J et al (1999) Perturbation to the lithosphere along the hotspot track of La Reunion from an offshore-onshore seismic transect. J Geophys Res 104:2895–2908

Garcia MO, Caplan-Auerbach J, De Carlo EH, Kurz MD, Becker N (2006) Geology, geochemistry and earthquake history of Loihi Seamount, Hawaii's youngest volcano. Chem Erde 66:81–108

Geist DJ, McBirney AR, Duncan RA (1986) Geology and petrogenesis of lavas from San Cristobal Island, Galapagos Archipelago. Geol Soc Am Bull 97:555–566

Geist D, White WM, Albarede F, Harpp K, Reynolds R, Blichert-Toft J et al (2002) Volcanic evolution in the Galapagos: the dissected shield of Volcan Ecuador. Geochem Geophys Geosyst 3:1061. https://doi.org/10.1029/2002GC000355

Geist D, Diefenbach AB, Fornari DJ, Kurz MD, Harpp K, Blusztajn J (2008) Construction of the Galapagos platform by large submarine volcanic terraces. Geochem Geophys Geosyst 9:Q03015. https://doi.org/10.1029/2007GC001795

Geist DJ, Bergantz G, Chadwick WW (2014) Galápagos Magma chambers. In: Harpp KS, Mittelstaedt E, d'Ozouville N, Graham DW (eds) The Galápagos: a natural laboratory for the earth sciences. AGU Geophys Monogr 204:55–69

Geldmacher J, van den Bogaard P, Hoernle K, Schmincke HU (2000) The $^{40}Ar/^{39}Ar$ age dating of the Madeira Archipelago and hotspot track (eastern North Atlantic). Geochem Geophys Geosyst 1:1008. https://doi.org/10.1029/1999GC000018

Geldmacher J, Hoernle K, Bogaard PVD, Duggen S, Werner R (2005) New $^{40}Ar/^{39}Ar$ age and geochemical data from seamounts in the Canary and Madeira volcanic provinces: support for the mantle plume hypothesis. Earth Planet Sci Lett 237:85–101

Genske FS, Turner SP, Beier C, Scaefer BF (2012) The petrology and geochemistry of Lavas from the Western Azores Islands of Flores and Corvo. J Petrol 53:1673–1708

Gente P, Dyment J, Maia M, Goslin J (2003) Interaction between the Mid-Atlantic Ridge and the Azores hot spot during the last 85 Myr: emplacement and rifting of the hot spot-derived plateaus. Geochem Geophys Geosyst 4:8514. https://doi.org/10.1029/2003GC000527

Gillot PY, Lefevre JC, Nativel PE (1994) Model for the structural evolution of the volcanoes of Reunion Island. Earth Planet Sci Lett 122:291–302

Gonzalez-Ferran O, Mazzuoli R, Lahsen A (2004) Geologia del complejo volcanico Isla de Pascua Rapa Nui. Scale 1:30,000. Santiago Chile Centro de Estudios Volcanologicos

Gourgaud A, Vincent P (2004) Petrology of two continental alkaline intraplate series at Emi Koussi volcano, Tibesti, Chad. J Volcanol Geoth Res 129:261–290

Guillou H, Carracedo JC, Paris R, Perez Torrado FJ (2004) Implications for the early shield-stage evolution of Tenerife from K/Ar ages and magnetic stratigraphy. Earth Planet Sci Lett 222:599–614

Guiraud R, Doumnang JC, Baigane M, Carretier S, Dominguez S (2000) Evidence for a 6000 km length NW-SE striking lineament in northern Africa: the Tibesti lineament. J Geol Soc London 157:897–900

Haase KM, Stoffers P, Garbe-Schoenberg CD (1997) The petrogenetic evolution of lavas from Easter Island and neighboring seamounts, near-ridge hotspot volcanoes in the SE Pacific. J Petrol 38:785–813

Haase KM (2002) Geochemical constraints on magma sources and mixing processes in Easter Microplate (SE Pacific): a case study of plume-ridge interaction. Chem Geol 182:335–355

Harpp KS, Wirth KR, Korich DJ (2002) Northern Galapagos Province: Hotspot-induced, near-ridge volcanism at Genovesa Island. Geology 30:399–402

Harpp KS, Fornari DJ, Geist DJ, Kurz MD (2003) Genovesa Submarine Ridge: a manifestation of plume-ridge interaction in the northern Galapagos Islands. Geochem Geophys Geosyst 4:8511. https://doi.org/10.1029/2003GC000531

Harpp KS, Geist DJ (2018) The evolution of Galápagos volcanoes: an alternative perspective. Front Earth Sci 6:50. https://doi.org/10.3389/feart.2018.00050

Harrison LN, Weis D, Garcia MO (2017) The link between Hawaiian mantle plume composition, magmatic flux, and deep mantle geodynamics. Earth Planet Sci Lett 463:298–309

Hildenbrand A, Marques FO, Catalão J, Catita CMS, Costa ACG (2012) Large-scale active slump of the southeastern flank of Pico Island, Azores. Geology 40:939–942

Hildenbrand A, Marques FO, Catalao J (2018) Large-scale mass wasting on small volcanic islands revealed by the study of Flores Island (Azores). Sci Rep 8:13898. https://doi.org/10.1038/s41598-018-32253-0

Hoernle K, Carracedo JC (2009) Canary Islands, Geology. In: Gillespie R, Clague D (eds) Encyclopedia of Islands 140

Huang HH, Lin F-C, Schmandt B, Farrell J, Smith RB, Tsai VC (2015) The Yellowstone magmatic system from the mantle plume to the upper crust. Science 348:773–776

Huppert KL, Royden LH, Perron JT (2015) Dominant influence of volcanic loading on vertical motions of the Hawaiian Islands. Earth Planet Sci Lett 418:149–171

Keppie JD, Dostal J, Murphy JB (2010) Complex geometry of the Cenozoic magma plumbing system in the central Sahara, NW Africa. Int Geol Rev 1:1–17. https://doi.org/10.1080/00206814.2010.496211

King SD, Adam C (2014) Hotspot swells revisited. Phys Earth Planet Inter 235:66–83

Knott TR, Branney MJ, Reichow MK, Finn DR, Tapster S, Coe RS (2020) Discovery of two new super-eruptions from the Yellowstone hotspot track (USA): is the Yellowstone hotspot waning? Geology 48:934–938

Koppers AAP, Staudigel H, Pringle MS, Wijbrans JR (2003) Short-lived and discontinuous intraplate volcanism in the South Pacific: hot spots or extensional volcanism? Geochem Geophys Geosyst 4:1089. https://doi.org/10.1029/2003GC000533

Krastel S, Schmincke HU, Jacobs CJ, Rihm R, Le Bas TP, Alibes B (2001) Submarine landslides around the Canary Islands. J Geophys Res 106:3977–3997

Langenheim VAM, Clague DA (1987) Stratigraphic framework of volcanic rocks of the Hawaiian Islands. US Geol Surv Prof Pap 1350:55–83

Larrea P, Franca Z, Widom E, Lago M (2018) Petrology of the Azores Islands. In: Kueppers U, Beier C (eds) Volcanoes of the Azores. Active volcanoes of the world. Springer, Germany, pp 197–249

Lenat JF, Vincent P, Bachelery P (1989) The off-shore continuation of an active basaltic volcano: Piton de la Fournaise (Reunion Island, Indian Ocean); structural and geomorphological interpretation from sea beam mapping. J Volcanol Geoth Res 36:1–36

Lenat JF, Gibert-Malengrau B, Galdeano A (2001) A new model for the evolution of the volcanic island of Reunion (Indian Ocean). J Geophys Res 106:8645–8663

Lipman PW, Sisson TW, Coombs ML, Calvert A, Kimura JI (2006) Piggyback tectonics: long-term growth of Kilauea on the south flank of Mauna Loa. J Volcanol Geoth Res 151:73–108

Lipman PW, Calvert AT (2011) Early growth of Kohala volcano and formation of long Hawaiian rift zones. Geology 39:659–662

Lipman PW, Calvert AT (2013) Modeling volcano growth on the Island of Hawaii: deep-water perspectives. Geosphere 9:1348–1383

Lodge A, Nippress SEJ, Rietbrock A, Garcia-Yeguas A, Ibanez JM (2012) Evidence for magmatic underplating and partial melt beneath the Canary Islands derived using teleseismic receiver functions. Phys Earth Planet Inter 212–213:44–54

Lourenço N, Miranda JM, Luis JF, Ribeiro A, Mendes Victor LA, Madeira J et al (1998) Morpho-tectonic analysis of the Azores Volcanic Plateau from a new bathymetric compilation of the area. Mar Geophys Res 20:141–156

Madeira J, Ribeiro A (1990) Geodynamic models for the Azores triple junction: a contribution from tectonics. Tectonophysics 184:405–415

Madeira J, Brum da Silveira A (2003) Active tectonics and first paleoseismological results in Faial, Pico and S. Jorge islands (Azores, Portugal). Ann Geophys 46:733–761

Madureira P, Moreira M, Mata J, Nunes JC, Gautheron C, Lorenco N et al (2014) Helium isotope systematics in the vicinity of the Azores triple junction: constraints on the Azores geodynamics. Chem Geol 372:62–71

Marques FO, Catalao JC, DeMets C, Costa ACG, Hildebrand A (2013) GPS and tectonic evidence for a diffuse plate boundary at the Azores Triple Junction. Earth Planet Sci Lett 381:177–187

Marques FO, Hildenbrand A, Costa ACG, Sibrant ALR (2020) The evolution of Santa Maria Island in the context of the Azores Triple Junction. Bull Volcanol 82:39

Martì J (2019) Las Cañadas caldera, Tenerife, Canary Islands: a review, or the end of a long volcanological controversy. Earth Sci Rev 196:102889

Martì J, Ortiz R, Gottsmann J, Garcia A, De la Cruz-Reyna S (2009) Characterising unrest during the reawakening of the central volcanic complex on Tenerife, Canary Islands, 2004–2005, and implications for assessing hazards and risk mitigation. J Volcanol Geoth Res 182:23–33

Martinez Arevalo C, de Lis MF, Hellfrich G, Garcia A (2013) Seismic evidence of a regional sublithospheric low velocity layer beneath the Canary Islands. Tectonophysics 608:586–599

Masson DG, Le Bas TP, Grevemeyer I, Weinrebe W (2008) Flank collapse and large-scale landsliding in the Cape Verde Islands, off West Africa. Geochem Geophys Geosyst 9:Q07015. https://doi.org/10.1029/2008GC001983

McCurry M, Rodgers DW (2009) Mass transfer along the Yellowstone hotspot track I: petrologic constraints on the volume of mantle-derived magma. J Volcanol Geoth Res 188:86–98

McQuarrie N, Rodgers DW (1998) Subsidence of a volcanic basin by flexure and crustal flow: the eastern Snake River Plain, Idaho. Tectonics 17:203–220

Mendes VB, Madeira J, Brum da Silveira A, Trota A, Elosegui P, Pagarete J (2013) Present-day deformation in Sao Jorge Island, Azores, from episodic GPS measurements (2001–2011). Adv Space Res 51:1581–1592

Merle O, Lenat JF (2003) Hybrid collapse mechanism at Piton de la Fournaise volcano, Reunion Island, Indian Ocean. J Geophys Res 108:2166. https://doi.org/10.1029/2002JB002014

Merle O, Mairine P, Michon L, Bachelery P, Smietana M (2010a) Calderas, landslides and paleo-canyons on Piton de la Fournaise volcano (La Réunion Island, Indian Ocean). J Volcanol Geoth Res 189:131–142

Merle O, Barde-Cabusson S, van Wyk deVries B (2010b) Hydrothermal calderas. Bull Volcanol 72:131–147

Michon L, Saint-Ange F, Bachelery P, Villeneuve N, Stadaucher T (2007) Role of the structural inheritance of the oceanic lithosphere in the magmato-tectonic evolution of Piton de la Fournaise volcano (La Reunion Island). J Geophys Res 112:B04205. https://doi.org/10.1029/2006JB004598

Michon L, Saint-Ange F (2008) Morphology of Piton de la Fournaise basaltic shield volcano (La Reunion Island): Characterization and implication in the volcano evolution. J Geophys Res 113:B03203. https://doi.org/10.1029/2005JB004118

Michon L, Villeneuve N, Catry T, Merle O (2009) How summit calderas collapse on basaltic volcanoes: New insights from the April 2007 caldera collapse of Piton de la Fournaise volcano. J Volcanol Geoth Res 184:138–151

Miller DS, Smith RB (1999) P and S velocity structure of the Yellowstone volcanic field from local earthquake and controlled-source tomography. J Geophys Res 104:15105–15121

Mitchell NC, Masson DG, Watts AB, Gee MJR, Urgeles R (2002) The morphology of the submarine flanks of volcanic ocean islands: a comparative study of the Canary and Hawaiian hotspot islands. J Volcanol Geoth Res 115:83–107

Moore JG (1987) Subsidence of the Hawaiian Ridge. US Geol Surv Prof Pap 1350:85–99

Moore JG, Clague DA (1992) Volcano growth and evolution of the island of Hawaii. Geol Soc Am Bull 104:1471–1484

Moore RB (1990) Volcanic geology and eruption frequency, Sao Miguel, Azores. Bull Volcanol 52:602–614

Moreira MA, Geoffroy L, Pozzi JP (2015) Magma flow pattern in dykes of the Azores revealed by anisotropy of magnetic susceptibility. J Geophys Res 120:662–690

Morriss MC, Karlstrom L, Nasholds MWM, Wolff JA (2020) The Chief Joseph dike swarm of the Columbia River flood basalts, and the legacy data set of William H. Taubeneck. Geosphere 16:1–25

Mouginis-Mark P, Rowland SK, Garbeil H (1996) Slopes of western Galapagos volcanoes from airborne interferometric radar. Geophys Res Lett 23:3767–3770

Naar DF, Hey RN (1991) Tectonic evolution of the Easter Microplate. J Geophys Res 96:7961–7993

Naumann T, Geist D (2000) Physical volcanology and structural development of Cerro Azul Volcano, Isabela Island, Galapagos: implications for the development of Galapagos-type shield volcanoes. Bull Volcanol 61:497–514

Navarro A, Lourenco N, Chorowicz J, Miranda JM, Catalao J (2009) Analysis of geometry of volcanoes and faults in Terceira Island (Azores): evidence for reactivation tectonics at the EUR/AFR plate boundary in the Azores triple junction. Tectonophysics 465:98–113

Neal CA, Brantley SR, Antolik L, Babb JL, Burgess M, Calles K et al (2019) The 2018 rift eruption and summit collapse of Kīlauea Volcano. Science 363:367–374

Nkono C, Liegeois J-P, Demaiffe D (2018) Relationships between structural lineaments and Cenozoic volcanism, Tibesti swell, Saharan metacraton. J Afr Earth Sci 145:274–283

Nunes JC, Camacho A, Franca Z, Montesinos FG, Alves M, Vieira R et al (2006) Gravity anomalies and crustal signature of volcano-tectonic structures of Pico Island (Azores). J Volcanol Geoth Res 156:55–70

O'Connor JM, Stoffers P, McWilliams MO (1995) Time-space mapping of Easter Chain volcanism. Earth Planet Sci Lett 136:197–212

O'Neill C, Muller D, Steinberger B (2003) Geodynamic implications of moving Indian Ocean hotspots. Earth Planet Sci Lett 215:151–168

Obrebski M, Allen RM, Xue M, Hung SH (2010) Slab-plume interaction beneath the Pacific Northwest. Geophys Res Lett 37:L14305. https://doi.org/10.1029/2010GL043489

Oehler JF, Labazuy P, Lenat JF (2004) Recurrence of major flank landslides during the last 2 Ma history of Reunion Island. Bull Volcanol 66:585–598

Okubo C, Benz HM, Chouet BA (1997) Imaging the crustal magma sources beneath Mauna Loa and Kilauea volcanoes, Hawaii. Geology 25:867–870

Pagarete J, Pinto JT, Mendes VB, Autunes C, Ribeiro H (1998) The importance of classical geodetic observations for analyzing the geodynamic behaviour of the Azores archipelago. Tectonophysics 294:281–290

Park J, Rye DM (2019) Why is crustal underplating beneath many hot spot islands anisotropic? Geochem Geophys Geosyst 20:4779–4809

Parsons T, Thompson GA, Smith RP (1998) More than one way to stretch: a tectonic model for extension along the plume track of the Yellowstone hotspot and adjacent Basin and Range Province. Tectonics 17:221–234

Payne S, McCaffrey R, King RW, Kattenhorn SA (2012) A new interpretation of deformation rates in the Snake River Plain and adjacent basin and range regions based on GPS measurements. Geophys J Int 189:101–122

Peltier A, Bachelery P, Staudacher T (2009) Magma transport and storage at Piton de La Fournaise (La Réunion) between 1972 and 2007: a review of geophysical and geochemical data. J Volcanol Geoth Res 184:93–108

Peng X, Humphreys ED (1998) Crustal velocity structure across the eastern Snake River Plain and the Yellowstone swell. J Geophys Res 103:7171–7186

Permenter JL, Oppenheimer C (2007) Volcanoes of the Tibesti massif (Chad, northern Africa). Bull Volcanol 69:609–626

Peterson DW, Moore RB (1987) Geologic history and evolution of geologic concepts. Island of Hawaii. US Geol Surv Prof Pap 1350:149–189

Pierce KL, Morgan LA (2009) Is the track of the Yellowstone hotspot driven by a deep mantle plume? review of volcanism, faulting, and uplift in light of new data. J Volcanol Geoth Res 188:1–25

Pik R, Marty B, Hilton DR (2006) How many mantle plumes in Africa? The geochemical point of view. Chem Geol 226:100–114

Poland M (2014) Contrasting volcanism in Hawaii and the Galápagos. In: Harpp KS, Mittelstaedt E, d'Ozouville N, Graham DW (eds) The Galápagos: a natural laboratory for the earth sciences. AGU geophysical monograph, vol 204, pp 5–26

Poland M, Miklius A, Montgomery-Brown EK (2014) Magma supply, storage, and transport at shield-stage Hawaiian volcanoes. In: Poland MP, Takahashi TJ, Landowski CM (eds) Characteristics of Hawaiian volcanoes. US geological survey professional paper, vol 1801, pp 179–236

Prono E, Battaglia J, Monteiller V, Got JL, Ferrazzini V (2009) P-wave velocity structure of Piton de la Fournaise volcano deduced from seismic data recorded between 1996 and 1999. J Volcanol Geoth Res 184:49–62

Ray JS, Mahoney JJ, Duncan RA, Ray J, Wessel P, Naar DF (2012) Chronology and geochemistry of Lavas from the Nazca Ridge and Easter Seamount chain: a 30 Myr Hotspot Record. J Petrol 53:1417–1448

Roberts GG, White N (2010) Estimating uplift rate histories from river profiles using African examples. J Geophys Res 115:B02406. https://doi.org/10.1029/2009JB006692

Robinson JE, Eakins BW (2006) Calculated volumes of individual shield volcanoes at the young end of the Hawaiian Ridge. J Volcanol Geoth Res 151:309–317

Romer RHW, Beier C, Haase KM, Hübscher C (2018) Correlated changes between volcanic structures and magma composition in the faial volcanic system, Azores. Front Ear Sci 6:78. https://doi.org/10.3389/feart.2018.00078

Rowland SK, Munro DC, Perez-Oviedo V (1994) Volcan Ecuador, Galapagos Islands: erosion as a possible mechanism for the generation of steep-sided basaltic volcanoes. Bull Volcanol 56:271–283

Rusby RI, Searle RC (1995) A history of the easter microplate, 5.25 Ma to present. J Geophys Res 100:12617–12640

Rychert CA, Laske G, Harmon N, Shearer PM (2013) Seismic imaging of melt in a displaced Hawaiian plume. Nat Geosci 6:657–660

Rychert CA, Harmon N, Ebinger C (2014) Receiver function imaging of lithospheric structure and the onset of melting beneath the Galápagos Archipelago. Earth Planet Sci Lett 388:156–165

Schmandt B, Dueker K, Humpreys E, Hansen S (2012) Hot mantle upwelling across the 660 beneath Yellowstone. Earth Planet Sci Lett 331–332:224–236

Searle R (1980) Tectonic pattern of the Azores spreading centre and triple junction. Earth Planet Sci Lett 51:415–434

Searle RC, Bird RT, Rusby RI, Naar DF (1993) The development of two oceanic microplates: Easter and Juan Fernadez microplates, East Pacific Rise. Geol Soc London 150:965–976

Sebai A, Stutzamnn E, Montagner J-P, Sicilia D, Beucler E (2006) Anisotropic structure of the African upper mantle from Rayleigh and Love wave tomography. Phys Earth Planet Inter 155:48–62

Sharp WD, Clague DA (2006) 50-Ma initiation of Hawaiian-Emperor bend records major change in Pacific plate motion. Science 313:1281–1284

Sibrant ALR, Hildebrand A, Marques FO, Weiss B, Boulesteix T, Hubscher C et al (2015) Morphostructural evolution of a volcanic island developed inside an active oceanic rift: S. Miguel Island (Terceira Rift, Azores). J Volcanol Geoth Res 301:90–106

Sichoix L, Bonneville A, McNutt MK (1998) The seafloor swells and Superswell in French Polynesia. J Geophys Res 103:27123–27133

Silva PF, Henry B, Marques FO, Hildebrand A, Madureira P, Meriaux CA et al (2012) Palaeomagnetic study of a subaerial volcanic ridge (Sao Jorge Island, Azores) for the past 1.3 Myr: evidence for the Cobb Mountain Subchron, volcano flank instability and tectonomagmatic Implications. Geophys J Int 188:959–978

Simkin T, Howard KA (1970) Caldera Collapse in the Galapagos Islands, 1968. Science 169:429–437

Sinton CW, Christie DM, Duncan RA (1996) Geochronology of Galapagos seamounts. J Geophys Res 101:13689–13700

Sinton CW, Hauff F, Hoernle K, Werner R (2018) Age progressive volcanism opposite Nazca plate motion: Insights from seamounts on the northeastern margin of the Galapagos Platform. Lithos 310–311:342–354

Smith RB, Braile LW (1994) The Yellowstone hotspot. J Volcanol Geoth Res 61:121–187

Smith RB, Jordan M, Steinberger M, Puskas CM, Farrell J, Waite G et al (2009) Geodynamics of the Yellowstone hotspot and mantle plume: Seismic and GPS imaging, kinematics, and mantle flow. J Volcanol Geoth Res 188:26–56

Spieker K, Rondenay S, Ramalho R, Thomas C, Helffrich G (2018) Constraints on the structure of the crust and lithosphere beneath the Azores Islands from teleseismic receiver functions. Geophys J Int 213:824–835

Staudacher T, Allegre CJ (1993) Ages of the second caldera of Piton de la Fournaise volcano (Reunion) determined by cosmic ray produced ^{3}He and ^{21}Ne. Earth Planet Sci Lett 119:395–404

Stillmann CJ (1999) Giant Miocene landslides and the evolution of Fuerteventura, Canary Islands. J Volcanol Geoth Res 94:89–104

Stock MJ, Bagnardi M, Neave DA, Maclennan J, Bernard B, Buisman I et al (2018) Integrated petrological and geophysical constraints on magma system architecture in the western Galápagos Archipelago: insights from Wolf volcano. Geochem Geophys Geosyst 19:4722–4743

Stoffers P, Hekinian R, Haase KM, Sonne Cruise SO-80 Scientific Party (1994) Geology of young submarine volcanoes west of Easter Island, Southeast Pacific. Mar Geol 118:177–185

Suetsugu D, Isse T, Tanaka S, Obayashi M, Shiobara H, Sugioka H et al (2009) South Pacific mantle plumes imaged by seismic observation on islands and seafloor. Geochem Geophys Geosyst 10:Q11014. https://doi.org/10.1029/2009GC002533

Swanson D, Duffield WA, Fiske RS (1976) Displacement of the South Flank of Kilauea Volcano: the result of forceful intrusion of magma into the rift zones. US geological survey professional paper, vol 963, 44 pp

Thordarson T, Garcia MO (2018) Variance of the flexure model predictions with rejuvenated volcanism at Kılauea point, Kauai, Hawaii. Front Ear Sci 6:121. https://doi.org/10.3389/feart.2018.00121

Tian Y, Zhao D (2012) P-wave tomography of the western United States: insight into the Yellowstone hotspot and the Juan de Fuca slab. Phys Earth Planet Inter 200–201:72–84

Trippanera D, Porreca M, Ruch J, Pimentel A, Acocella V, Pacheco J et al (2014) Relationships between tectonics and magmatism in a transtensive/transform setting: an example from Faial Island (Azores, Portugal). Geol Soc Am Bull 126:164–181

Trota A, Houliè N, Briole P, Gaspar JL, Sigmundsson F, Keigl KL (2006) Deformation studies at Furnas and Sete Cidades Volcanoes (Sao Miguel Island, Azores). Velocities and further investigations. Geophys J Int 166:952–956

Vezzoli L, Acocella V (2009) Easter Island, SE Pacific: an end-member type of hotspot volcanism. Geol Soc Am Bull 121:869–886

Vidal V, Bonneville A (2004) Variations of the Hawaiian hot spot activity revealed by variations in the magma production rate. J Geophys Res 109:B03104. https://doi.org/10.1029/2003JB002559

Villagomez DR, Toomey DR, Geist DJ, Hooft EEE, Solomon SC (2014) Mantle flow and multistage melting beneath the Galápagos hotspot revealed by seismic imaging. Nat Geosci 7:151–156

Vogt PR, Jung WY (2004) The Terceira Rift as hyper-slow, hotspot-dominated oblique spreading axis: a comparison with other slow-spreading plate boundaries. Earth Planet Sci Lett 218:77–90

Walker GPL (1987) The dike complex of Koolau Volcano, Oahu: internal structure of a Hawaiian rift zone. US Geol Surv Prof Pap 1350:961–997

Walter TR, Troll VR, Cailleau B, Belousov A, Schmincke HU, Amelung F et al (2005) Rift zone reorganization through flank instability in ocean island volcanoes: an example from Tenerife, Canary Islands. Bull Volcanol 67:281–291

Walter TR, Klugel A, Munn S (2006) Gravitational spreading and formation of new rift zones on overlapping volcanoes. Terra Nova 18:26–33

Wang K, MacArthur HS, Johanson I, Montgomery-Brown EK, Poland MP, Cannon EC et al (2019) Interseismic quiescence and triggered slip of active normal faults of Kīlauea Volcano's south flank during 2001–2018. J Geophys Res 124:9780–9794

Watts AB, Peirce C, Collier J, Dalwood R, Canales JP, Henstock TJ (1997) A seismic study of lithospheric flexure in the vicinity of Tenerife, Canary Islands. Earth Planet Sci Lett 146:431–447

Wauthier C, Roman DC, Poland MP (2019) Modulation of seismic activity in Kīlauea's upper East Rift Zone (Hawaii) by summit pressurization. Geology 47:820–824

Weis D, Garcia MO, Rhodes JM, Jellinek M, Scoates JS (2011) Role of the deep mantle in generating the compositional asymmetry of the Hawaiian mantle plume. Nat Geosci 4:831–838

Werner R, Hoernie K, Barckhausen U, Hauff F (2003) Geodynamic evolution of the Galapagos hot spot system (Central East Pacific) over the past 20 m.y.: Constraints from morphology, geochemistry, and magnetic anomalies. Geochem Geophys Geosyst 4:1108. https://doi.org/10.1029/2003GC000576

Wolfe CJ, Solomon SC, Laske G, Collins JA, Detrick RS, Orcutt JA et al (2009) Beneath the Hawaiian hot spot. Science 326:1388–1390

Wolff JA, Ramos FC, Hart GL, Patterson JD, Brandon AD (2008) Columbia River flood basalts from a centralized crustal magmatic system. Nat Geosci 1:177–180

Wotzlaw J-F, Bindeman IN, Stern RA, D'Abzac F-X, Schaltegger U (2015) Rapid heterogeneous assembly of multiple magma reservoirs prior to Yellowstone supereruptions. Sci Rep 5:14026. https://doi.org/10.1038/srep14026

Xue M, Allen RM (2007) The fate of the Juan de Fuca plate: Implications for a Yellowstone plume head. Earth Planet Sci Lett 264:266–276

Yang T, Shen Y, van der Lee S, Solomon SC, Hung SH (2006) Upper mantle structure beneath the Azores hotspot from finite-frequency seismic tomography. Earth Planet Sci Lett 250:11–26